The *Lotus japonicus* alpha Expansin *EXPA1* is recruited during intracellular and intercellular rhizobial colonization

Author names and affiliations:

Jesús Montiel[a,1], Ivette García Soto [a], Elizabeth Monroy Morales [a], Beatrice Lace [c], Mads Vestergaard [b], Niels Sandal [b], Thomas Ott [c], and Jens Stougaard [b,2]

[a]Centro de Ciencias Genómicas. UNAM. Cuernavaca, México

[b]Department of Molecular Biology and Genetics, Aarhus University, Denmark. DK-8000, Aarhus C, Denmark

[c]Cell Biology, Faculty of Biology, University of Freiburg, 79104 Freiburg, Germany

Correspondence: Jesús Montiel and Jens Stougaard

[1] jmontiel@ccg.unam.mx

[2] stougaard@mbg.au.dk

Significance statement:

The colonization of legume roots by rhizobia represents a critical phase in the establishment of root nodule symbiosis. In this study, we demonstrated that LjEXPA1, a plant protein involved in cell wall loosening, is indispensable in the two modalities of rhizobial symbiotic infection in *Lotus japonicus* roots.

ABSTRACT

Most legumes establish a mutualistic association with rhizobia, a group of nitrogen-fixing bacteria. In *Lotus japonicus*, the symbiotic colonization occurs intracellularly, via root-hair infection threads by *Mesorhizobium loti*, or intercellularly, with *Agrobacterium pusense* IRBG74. In both mechanisms, cell wall remodeling is presumably an essential process. In plants, alpha-Expansins (EXPA) promote cell wall loosening by non-enzymatically triggering a pH-dependent relaxation. In this study, we show that LjEXPA1, is critical for the intracellular and intercellular symbiotic program in *L. japonicus*. Promoter activity and subcellular localization analyses revealed that EXPA1 is recruited at essential compartments and structures of epidermal and cortical cells in both mechanisms of rhizobial infection, such as the infection chambers, infection pockets and transcellular infection threads. Additionally, EXPA1-YFP abundantly accumulated in dividing cortical cells during nodule formation. The expression profile of *EXPA1* correlates with the symbiotic phenotype observed in homozygous mutants disrupted in the *EXPA*1 gene (*expA1*-1 and *expA1*-2). Infection thread formation and intercellular colonization was drastically reduced in *expA1*-1 and *expA1*-2 mutants, respect to wild type plants. Similarly, nodule formation was significantly reduced in these mutants after *M. loti* or IRBG74 inoculation. Our results indicate that non-enzymatic cell wall remodeling by the alpha Expansin EXPA1 is crucial for the successful establishment of *Lotus*-rhizobia symbiosis, regardless of the infection mechanism.

INTRODUCTION

Nitrogen is a limiting macronutrient for plant growth; however, legumes can obtain it through an endosymbiotic relationship with nitrogen-fixing soil bacteria, known as rhizobia. This legume-rhizobial symbiosis leads to the formation of root-derived organs known as nodules (Downie, 2014). A successful symbiosis between legumes and rhizobia is initiated by a molecular dialogue, which requires two coordinated developmental processes: the bacterial infection in the epidermis, which allows bacteria to invade host cells, and the induction of cortical cell divisions, leading to the formation of nodule primordia (Oldroyd *et al.*, 2011, Lace and Ott, 2018). Although infection and organogenesis are highly synchronized, these are genetically separable processes. Nodulation requires host perception of lipochitooligosaccharide signals, known as Nod factors, which are synthesized by rhizobia in response to plant-derived flavonoids. In *Lotus japonicus*, Nod factors are recognized by two LysM receptor-like kinases, Nod Factor Receptor 1 (*Lj*NFR1) and *Lj*NFR5, which trigger a downstream signaling cascade (Radutoiu *et al.*, 2003, Bozsoki *et al.*, 2020, Rubsam *et al.*, 2023).

Rhizobial infection in legumes can occur via two primary routes: transcellular (infection thread (IT)-mediated) and intercellular (without epidermal infection threads). Intracellular entry is the best-known infection process particularly in model legumes like *Medicago truncatula* and *L. japonicus* (de Carvalho-Niebel *et al.*, 2024). In this process, rhizobia attach to elongating root hairs, inducing growth redirection and entrapment within a curl, forming an infection chamber (IC). From this chamber, the cell wall and plasma membrane invaginate to form an inward, transcellular tunnel-like structure, known as IT, to mediate the entry of rhizobia and guide their proliferation across root tissues (Gao *et al.*, 2024). Throughout the progression of rhizobial infection, organogenesis is executed in root cortical and pericycle cells, resulting in the development of a nodule primordium. As the infection threads transcellularly grow, they penetrate several cortical cell layers and release bacteria inside the nodule primordia cells (Monroy-Morales *et al.*, 2022). These colonized nodule cells create a low-oxygen environment that supports the activity of the nitrogenase complex in bacteroids, a bacterial enzyme that reduces atmospheric

nitrogen into ammonia, which plants can then assimilate through a process known as biological nitrogen fixation (Ferguson *et al.*, 2010).

Although the transcellular infection pathway is well-documented, approximately 25% of legume species undergo intercellular infection (Sprent *et al.*, 2017). In this infection mode, rhizobia enter the root through sites of epidermal cracking or fissures, followed by intercellular penetration. Species such as *Sesbania rostrata*, *Arachis hypogaea* (peanut), *Lupinus albus* and *Lotus uliginosus,* exhibit nodules infected without epidermal ITs (Ibañez *et al.*, 2017). Furthermore, *L. japonicus* can also be infected through both transcellular and intercellular routes (Quilbe *et al.*, 2022). While *L. japonicus* typically undergoes transcellular infection via ITs, some plant mutants lacking epidermal ITs can still form nodules and internalize rhizobia, albeit at a low frequency (Karas *et al.*, 2005, Madsen *et al.*, 2010). Additionally, certain strains of rhizobia, such as *Sinorhizobium fredii* HH103, *Rhizobium leguminosarum* Norway, and *Agrobacterium pusense* IRGB74, colonized *Lotus* roots intercellularly (Acosta-Jurado *et al.*, 2016, Liang *et al.*, 2019, Montiel *et al.*, 2021, Zarrabian *et al.*, 2022). This highlights the flexibility of *L. japonicus* in accommodating both infection routes depending on the rhizobial strain and environmental conditions.

A key aspect of rhizobial infection is cell wall remodeling, which is essential for allowing rhizobia to enter root cells and for the reactivation of meristematic activity during nodule development (Rich *et al.*, 2014). The plant cell wall is a dynamic structure, mainly composed by pectin, hemicellulose and cellulose, that can be altered in structure and composition by the action of a complex and sophisticated network of numerous protein families (Broxterman and Schols, 2018). Nonetheless, the evidence collected by different research groups indicates that certain members of these cell wall protein families have a pivotal role in the legume-rhizobia symbiosis. In *L. japonicus*, nodule development is negatively affected in the *cellulose synthase-like d1* mutant (Karas *et al.*, 2021), while in *M. truncatula* the *Glycoside Hydrolase 9C2 (GH9C2)* gene is required for both epidermal and nodule infection (Zhao *et al.*, 2025). Similarly, a nodulation pectate lyase gene (*NPL*) is induced in the nodulation process of *L. japonicus* after *M. loti* inoculation, and the *Ljnpl* mutant

exhibit empty nodules and abnormal root-hair ITs (Xie *et al.*, 2012). In *M. truncatula* root hairs, the coordinated action of a symbiosis-specific pectin methyl esterase (SyPME1) and MtNPL, allows intracellular progression of *Sinorhizobium meliloti* (Su *et al.*, 2023) and MtNPL was also shown to act synergistically with GH9C2 on rhizobial infection (Zhao *et al.*, 2025). *In vivo* localization of cell wall proteins, such as ENOD11, NPL, SyPME1 and GH9C2, has been observed at early infection sites, supporting cell wall remodeling in radially-expanding chambers to facilitate IT growth (de Carvalho-Niebel *et al.*, 2024). Remodeling may occur at the transcellular passage cleft (TPC), supporting cell-to-cell progression of the IT and resulting in the release of bacteria into dividing primordium cells (Roy *et al.*, 2020, Zhang and Ott, 2024).

The mechanical properties of the cell wall can be modified by the non-enzymatic action of Expansins, a large family of extracellular proteins with a carbohydrate binding module (Cosgrove, 2015). Expansins are classified into four subfamilies based on phylogenetic analysis and sequence characteristics: α-Expansin (EXPA), β-Expansin (EXPB), Expansin-like A (EXLA), and Expansin-like B (EXLB). Both α-expansins and β-expansins are well-known for their ability to relax the cell wall, aiding in processes like cell expansion during growth and development (Cosgrove, 2015). In the context of symbiosis, the overexpression of the soybean β-expansin *GmEXPB2*, enhances root growth, increases rhizobial infection events, promotes primordia formation, and boosts the number of mature nodules (Li *et al.*, 2015). However, the transcriptome analysis in different legumes revealed that during nodulation, the expression of several isoforms of the alpha Expansin subfamily are significantly induced (Gyorgyey *et al.*, 2000, Giordano and Hirsch, 2004, Libourel *et al.*, 2023). Herein to get further insights into the role of alpha Expansins in the Legume-rhizobia symbiosis, we analyzed *LjEXPA1* during the symbiotic program induced by *M. loti* and *A. pusense* IRBG74, that colonize *L. japonicus* roots, intra- and intercellularly, respectively.

MATERIALS AND METHODS

141 **Biological Materials and Nodulation Kinetics**

142

143 In this study, wild type and mutant lines belong to the genetic background of *L.*
144 *japonicus* accession Gifu (Handberg and Stougaard, 1992). The mutant lines
145 30015381 and 30164465 were obtained from the *LORE1* collection and genotyped,
146 as described in the database, to obtain homozygous mutants (Malolepszy *et al.*,
147 2016). The seeds were scarified with sandpaper, sterilized with a 5% chlorine
148 solution for 15 minutes and washed with sterile distilled water (3-5 times) to remove
149 any residual chlorine. The disinfected seeds were germinated in 12 cm x 12 cm
150 square Petri dishes containing 1.2% Bacto agar in a growth chamber at 21°C.
151 Seedlings at 3-7 days post-germination (dpg) were transferred to new square Petri
152 dishes containing ¼ B&D solid medium (Broughton and Dilworth, 1971) and filter
153 paper, and then placed in a growth room with photoperiod (16:8 at 21°C). For
154 nodulation kinetics, the seedlings were inoculated with 1 mL of *M. loti* R7A::DsRed,
155 *M. loti* R7A-GFP or IRBG74::DsRed (OD 600nm= 0.05), previously grown in YEM
156 medium. Nodule numbers were recorded at 1-6 weeks post-inoculation (wpi) using
157 a stereomicroscope.

158 **Phylogenetic Analysis**

159 To identify members of the Expansin superfamily in *Lotus*, BLASTP analyses were
160 performed using as queries the 42 annotated Expansin protein sequences from *M.*
161 *truncatula*. Homologous protein sequences were also retrieved from the Expansin
162 Gene Family Database (http://www.expansingenefamily.com) for the following
163 species: *Glycine soja* (*G. soja*) (Feng *et al.*, 2022), *Arabidopsis thaliana* (*A. thaliana*)
164 (https://www.arabidopsis.org), *Physcomitrium patens* (*P. patens*), *Oryza sativa* (*O.*
165 *sativa*), *Sorghum bicolor* (*S. bicolor*), Solanum pennellii (S. pennellii), *Capsella*
166 *rubella* (*C. rubella*), and *Phaseolus vulgaris* (*P. vulgaris*) (Kok *et al.*, 2023). Protein
167 sequences from *Lotus* and the ten additional species were aligned using ClustalX2
168 (Larkin *et al.*, 2007), and a phylogenetic tree was inferred by the Neighbor-Joining
169 method. Tree topology was evaluated, and the graphical representation of the tree

170 was edited and exported using the Interactive Tree of Life (iTOL) web interface
171 (https://itol.embl.de)
172
173 **Intercellular and intracellular rhizobial infection**
174 Gifu and *expA* mutant lines were inoculated with the *M. loti*–LacZ or IRBG74, as
175 described for nodulation kinetics. For intracellular infection, roots were collected at
176 10 dpi with *M. loti* and stained with a 2 mg/mL X-Gal solution to visualize and count
177 the epidermal and cortical ITs under an optical microscope. The intercellular infection
178 was analyzed as previously described by Montiel et al. (2021). Gifu and mutant roots
179 were collected at 3 weeks post-inoculation (wpi) with IRBG74, incubated for 1 min in
180 a solution for surface disinfection (0.3% *w*/*v* of hypochlorite and 70% *v*/*v* EtOH), and
181 then washed 5 times with distilled water. The total DNA was extracted from individual
182 roots, adjusted to a final concentration of 10 ng μL−1, and used as a template for
183 qPCR to evaluate the IRBG74 *NodA* abundance with the primers; forward:
184 GAACTGCAAGTTGACGATCACGC and reverse:
185 AAACGTCGTAACAAGCCCATGTGG. The expression values were normalized to
186 the abundance of the *L. japonicus* gene LotjaGi1g1v0152000.1 with the
187 oligonucleotides; forward: GAAGGACCCAGAGGATCACA and reverse:
188 CGGTCTTCGTACTTCTTCGC using the delta Ct method (Pfaffl, 2001).
189
190 **Constructs for promoter activity and subcellular localization**
191 For *pLjEXPA1::tYFP-nls*, and *pLjEXPA1::LjEXPA1-YFP_p35S::DsRed-nls*
192 constructs, the predicted promoter sequence (2 kb upstream of the start codon) and
193 coding sequence (CDS) were obtained from the *L. japonicus* Gifu genome in the
194 *Lotus* database. Each module was assembled using Golden Gate technology, and
195 the resulting constructs were used to transform *Agrobacterium rhizogenes* strain
196 AR1193. Subsequently, Gifu roots were transformed according to a standardized
197 protocol (Hansen *et al.*, 1989). Transgenic roots were inoculated with *M. loti* R7A-
198 DsRed (Kelly *et al.*, 2013) or IRBG74-DsRed (Montiel *et al.*, 2021), and examined
199 by confocal microscopy. For subcellular localization imaging, bacterial strains were

inoculated using an OD600 = 0.01 (*M. loti* R7A-DsRed) or OD600 = 0.005 (IRBG74-DsRed).

Confocal Microscopy Analysis

The first set of observations, focused on promoter activity, was made using an inverted confocal laser scanning microscope (FV1000) equipped with a 40×/NA 0.75 dry objective. YFP and DsRed signals were detected using excitation wavelengths of 488 nm and 543 nm, respectively, with emission windows set at 505-525 nm and 560-660 nm to collect their signal.

Subcellular localization imaging was performed using a Leica SP8 FALCON FLIM confocal microscope equipped with a 20 x/0.75 water immersion lens (Leica Microsystems, Mannheim, Germany). A pulsed White Light Laser (WLL) was used as an excitation source. YFP and DsRed were excited at 513 nm and 561 nm, respectively, and their emissions were collected at 520–550 nm and 580–620 nm. Before inoculating the bacterial strains, the position of the apex of transformed roots was marked on plates. At 4–5 dpi (M. loti R7A-DsRed) or 8-12 dpi (IRBG74-DsRed), root segments that had grown beyond the mark were excised, mounted in water, and imaged.

Statistical analyses

All statistical analyses were performed using GraphPad Prism 10, and graphical representations were made using R. Individual comparisons were done by Mann–Whitney *U* test. *P*-values and the number of samples are shown in the figure legends.

RESULTS

Two *Lotus* alpha *Expansins* are upregulated by *M. loti* and IRBG74

To investigate the potential role of *Lotus* Expansins in the legume-rhizobia symbiosis, we first performed a search in the *Lotus* genome for homologous genes to soybean and *Arabidopsis thaliana Expansins*, detecting 37 genes (Table S1). To narrow down the set of *Lotus* Expansins that are likely recruited during the symbiotic process, the expression profile of these sequences was explored in the Lotus Expression Atlas (Mun *et al.*, 2016, Kamal *et al.*, 2020). This analysis revealed that a relatively low number of Expansins are induced during root nodule symbiosis (RNS), or in root hairs, where intracellular rhizobial colonization occurs (Figure S1). To identify which isoforms might participate in the intracellular and intercellular infection program, a gene expression heatmap was made with the available RNA-seq data of *Lotus* roots inoculated with *M. loti* and IRBG74 (Montiel *et al.*, 2021). Only three Expansin were significantly induced by both symbionts at different timepoints: LotjaGi1g1v0089200, LotjaGi2g1v0429600 and LotjaGi1g1v0606600 (Figure 1A).

To obtain additional information of *Lotus* Expansins, the amino acid sequences for the 37 genes were predicted, and a phylogenetic tree was constructed. This analysis included the Expansin family of representative legumes (*Glycine soja*, *Phaseolus vulgaris* and *Medicago truncatula*) and non-legumes (*Oryza sativa* and *A. thaliana*) plant species. The resulting phylogenetic tree showed that for all species tested, the EXPA subfamily is the most abundant, followed by EXLB (Figure S2A and B). The phylogenetic distribution of the four *Lotus* Expansin subfamilies was also consistent with their clustering by an identity matrix (Figure S2C). In addition, this analysis revealed that one of the *Expansin* genes induced by *M. loti* and IRBG74, encodes an Alpha subfamily isoform (Figure 1C), hereafter referred as *EXPA1* (LotjaGi1g1v0089200). Interestingly, in the single cell RNA-seq data of *L. japonicus* roots at 10 days post-inoculation (dpi) with *M. loti*, *EXPA1* expression was primarily associated to cells colonized by rhizobia (Figure 1B). Despite the presence of numerous Expansin members in *Lotus*, the available expression data suggest, that *EXPA1* is the isoform mainly recruited both in the intra- and intercellular rhizobial

infection. Based on this evidence, we decided to focus on the analysis of *EXPA1* during the two modalities of rhizobial colonization in *Lotus*.

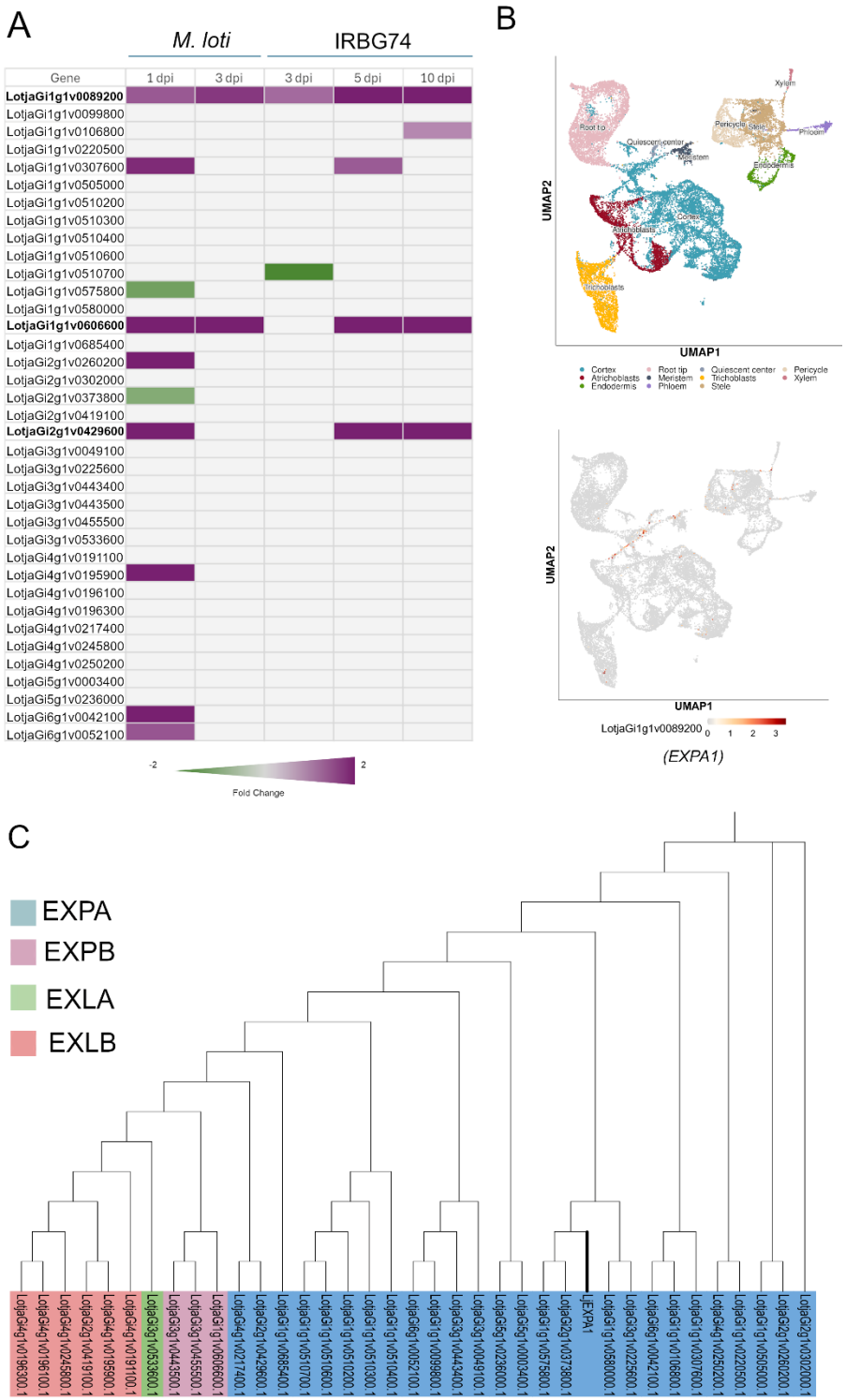

Figure 1. Expression profile and phylogeny of *Lotus* Expansins. **A,** Heat map expression of *Lotus* genes encoding Expansins in roots inoculated with *M. loti* and IRBG74

261 (extracted from RNAseq data; Montiel et al. 2021). **B,** Expression pattern of *LjExpA1*
262 (LotjaGi1g1v0089200) extracted from single-cell RNAseq data (Frank et al. 2023). **C,**
263 Phylogenetic distribution of *Lotus* Expansins across four subfamilies: alpha, beta, alpha-like,
264 and beta-like.

265

266 ***EXPA1* promoter activity is linked to rhizobial colonization and nodule**
267 **organogenesis**

268 To examine in more detail the spatial-temporal expression of *EXPA1* by confocal
269 microscopy, a 2 kb promoter sequence of this gene was fused to a nuclear-localized
270 triple YFP (*pEXPA1::tYFP-nls*). In uninoculated conditions, the *EXPA1* promoter was
271 strongly expressed at the root apex and emerging lateral root primordia, but it was
272 also occasionally detected in the elongation and, differentiation zone as well as in
273 root hairs (Figure 2A-C). In response to *M. loti* R7A inoculation, the *EXPA1* promoter
274 was expressed in deformed root hairs and neighboring epidermal cells, before the
275 initiation of rhizobial infection (Figure 2D). This expression pattern was maintained
276 during IT progression (Figure 2E). Similarly, the promoter activity of *EXPA1* was
277 detected at early steps of the intercellular colonization by IRBG74, such as in twisted
278 root hairs with infection pockets (IP) and in surrounding epidermal cells (Figure 2F).
279 These observations confirm that *EXPA1* is linked to intra- and intercellular
280 colonization events in *Lotus*. However, *EXPA1* also appears to be involved in the
281 nodule organogenesis program, since a prominent promoter expression was found
282 in dividing cortical cells during nodule development (Figure 2G and H).

283

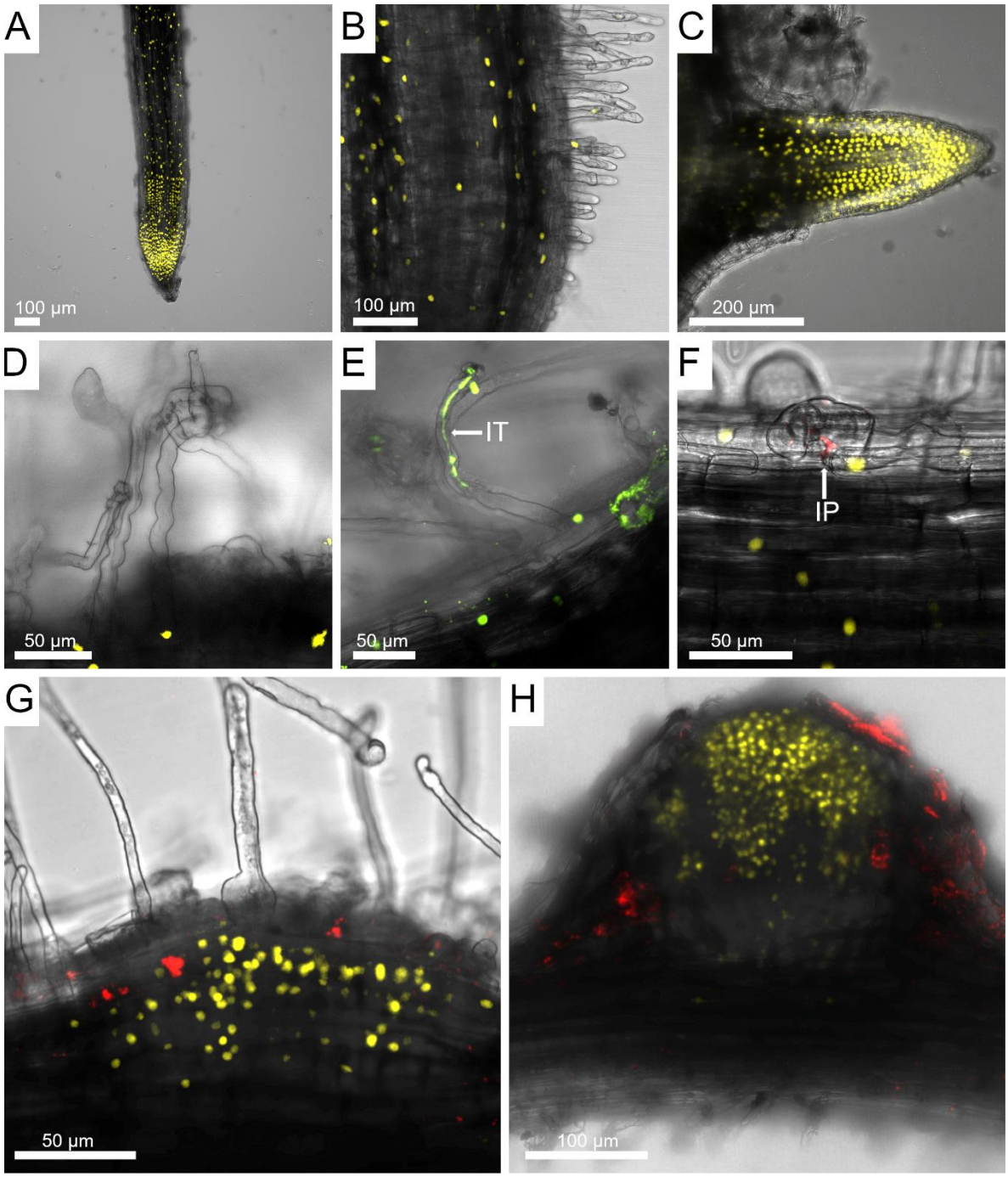

Figure 2. Promoter activity of *LjEXPA1* during intercellular and intracellular rhizobial infection. Confocal microscopy images of *Lotus* transgenic roots expressing the *pLjEXPA1*::*tYFP*-nls construct in uninoculated plants (**A-C**), and after inoculation with *M. loti*-DsRed **(D and E)** and IRBG74-DsRed **(F and H)**. IT, infection thread; IP, infection pocket.

290 **Subcellular localization of EXPA1 during intra- and intercellular rhizobial**
291 **colonization**
292 The spatial and temporal expression profile of *EXPA1* place it at critical steps and
293 tissues during the *Lotus*-rhizobia symbiosis. These observations prompted us to
294 explore the localization of this Expansin in *Lotus* roots during rhizobial colonization
295 and nodule development. For this purpose, a construct was generated to express
296 EXPA1 fused to YFP under the control of its native promoter together, with a
297 constitutive expression of a nuclear-localized DsRed as fluorescent transformation
298 marker: *pEXPA1::EXPA1-YFP_p35S::DsRed-nls*. During infection of transgenic
299 roots by *M. loti*-DsRed, EXPA1-YFP was enriched in the cell wall surrounding the
300 infection chamber (Figure 3A), whereas its presence was barely detectable in the IT
301 cell wall (Figure 3B). Interestingly, a very intense EXPA1-YFP accumulation was also
302 observed at the transcellular passage cleft (TPC), where the IT progresses from cell
303 to cell (Figure 3C).
304

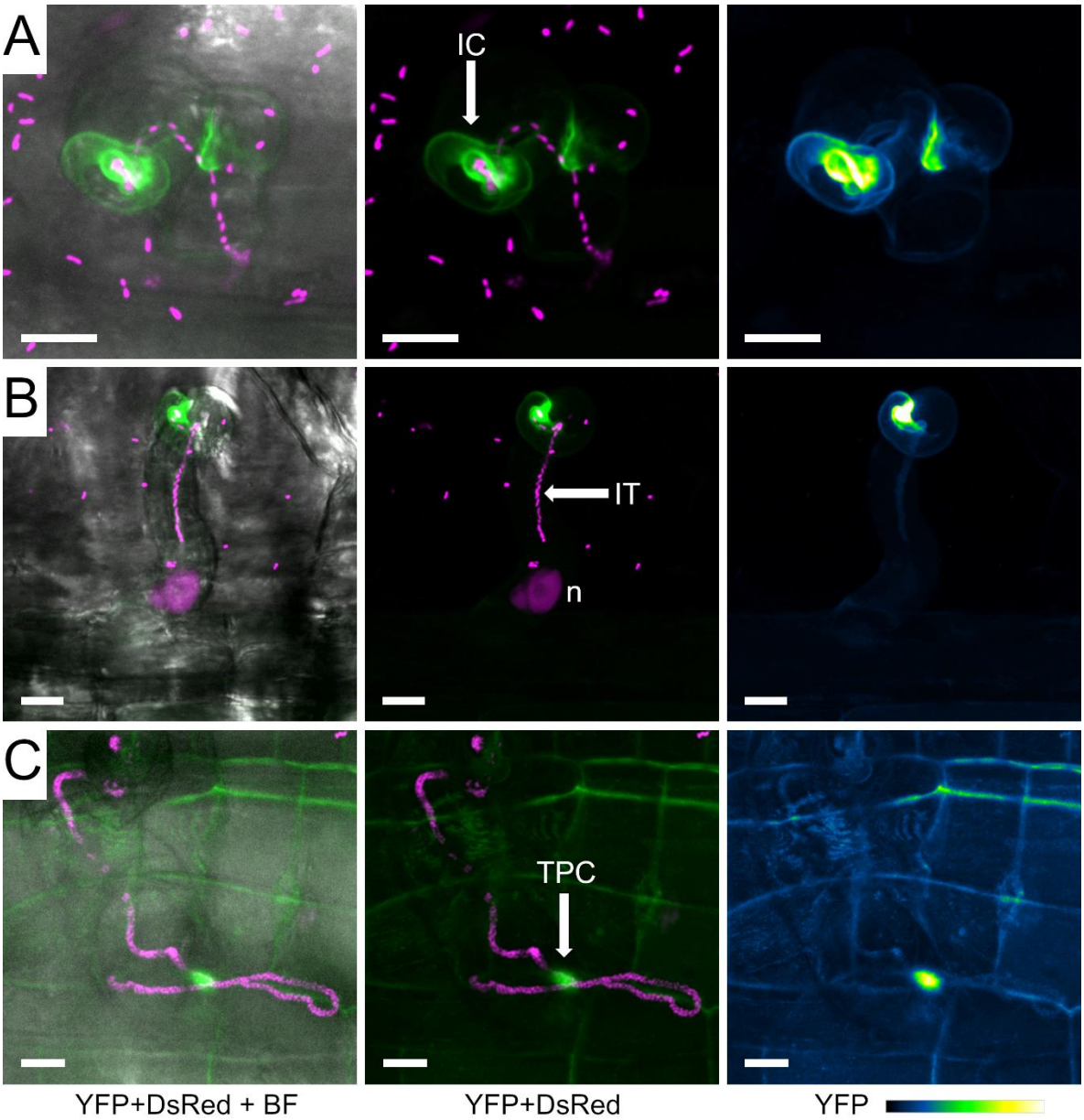

Figure 3. Subcellular localization of LjEXPA1 during intracellular rhizobial infection. Live-cell confocal images of Lotus transgenic roots expressing the *pEXPA1::EXPA1-YFP_p35S::DsRed-nls* construct at different stages of *M. loti* colonization: **A,** Infection chamber (IC) formation; **B,** Infection thread (IT) progression; **C,** Transcellular passage cleft (TPC). Images are maximum intensity projections of z-stacks (step size = 1 µm) showing either the merge of the YFP (green) and DsRed (magenta) channels with (left) or without (middle) the bright field (BF) channel, or the isolated YFP channel (green fire blue, right). At least twelve composite plants from two independent experiments were analyzed. IC = infection chamber; IT = infection thread; TPC = transcellular passage cleft. Scale = 10 µm.

316 In roots inoculated with IRBG74-DsRed, EXPA1-YFP was detected in specific zones
317 of the cell wall, of twisted root hairs containing infection pockets (IP), a structure that
318 precedes the intercellular colonization of IRBG74 (Figure 4A-C). Additionally,
319 EXPA1-YFP was abundantly recruited at the cell wall of dividing cortical cells during
320 nodule primordia formation after both *M. loti* R7A-DsRed and IRBG74-DsRed
321 inoculation (Figure S3). These results further confirm the relevant presence of
322 EXPA1 at key steps and cellular domains during the intra- and intercellular invasion
323 of *Lotus* roots by *M. loti* and IRBG74, respectively.

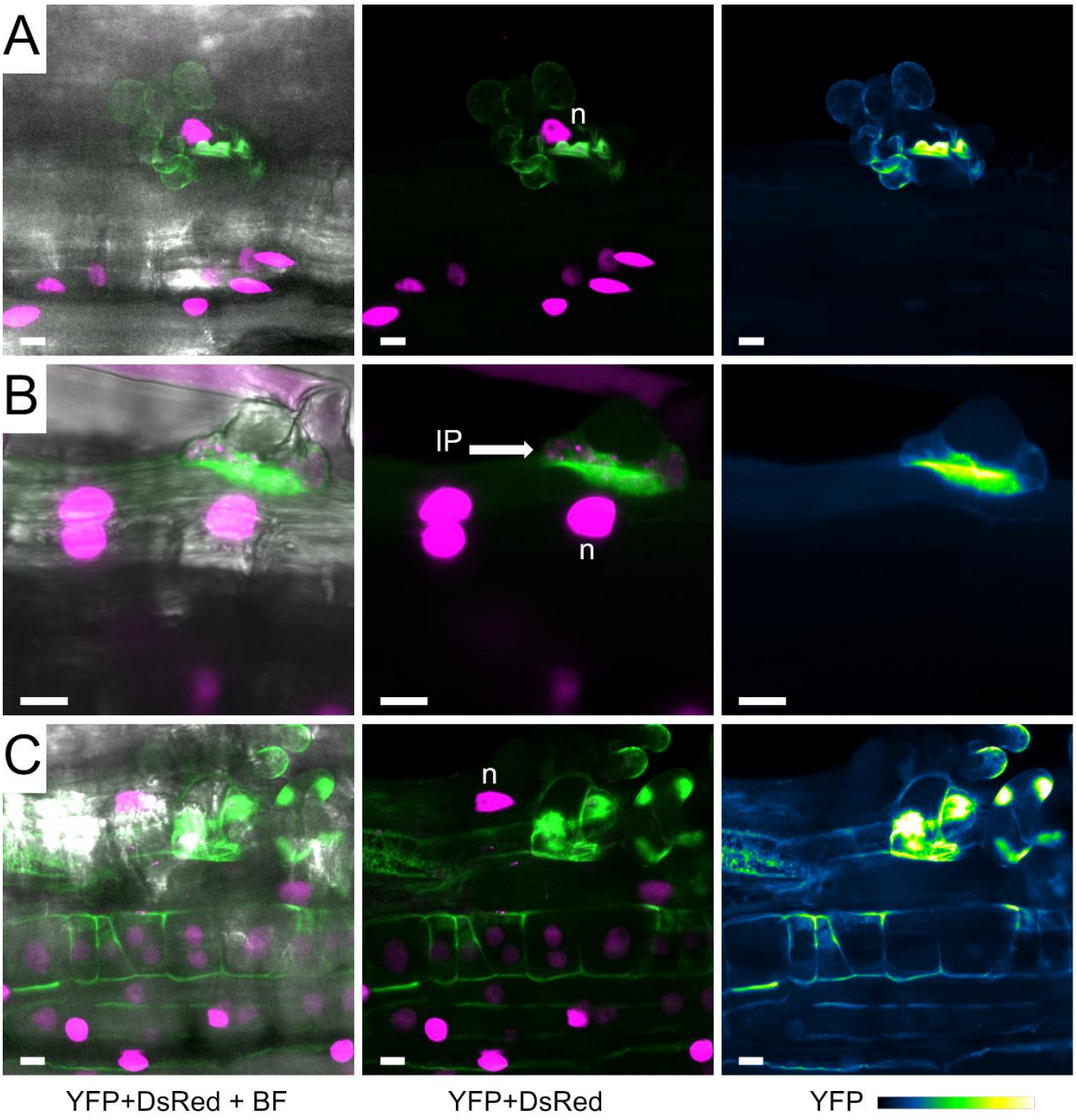

324

325 **Figure 4. Subcellular localization of LjEXPA1 during intercellular infection.** Live-cell
326 confocal images of *Lotus* transgenic roots expressing the *pEXPA1::EXPA1-*
327 *YFP_p35S::tDsRed-nls* construct at different steps of intercellular colonization by *A.*
328 *pusense* IRBG74-DsRed: **A** and **C**, Root hairs swelling and twisting; **B** and **C**, Infection
329 pocket formation (IP). Images are maximum intensity projections of z-stacks (step size = 1
330 µm) showing the merge of the YFP (green) and DsRed (magenta) channels with (left) or
331 without (right) the bright field (BF) channel. At least twelve composite plants from two
332 independent experiments were analyzed. IC = infection chamber; IT = infection thread; TPC
333 = transcellular passage cleft. Scale = 10 µm.

334

335

336 **Compromised intra- and intercellular symbiotic programs in *expA1* mutants**

337 To determine the relevance of *LjEXPA1* in the *Lotus*-rhizobia symbiosis, two
338 homozygous mutant lines were obtained from the *Lotus* retrotransposon (*LORE1*)
339 mutant collection (Mun *et al.*, 2016). *expA1*-1 and *expA1*-2 lines had retrotransposon
340 insertions in the last exon and the 3' UTR of *EXPA1*, respectively, leading to reduced
341 transcript levels (Figure S4). First, we evaluated the nodulation capacity of the
342 mutants upon inoculation with *M. loti* R7A, by recording their nodulation kinetics.
343 While on wild type Gifu roots (hereafter referred as Gifu), nodule primordia were
344 observed at 1 wpi with *M. loti* R7A, these structures only appeared at 2 wpi in the
345 mutants (Figure 5A). Besides the delay in nodule primordia formation, the nodule
346 numbers were significantly lower at 3-6 wpi in the mutants compared to Gifu wild
347 type plants (Figure 5A). Importantly, the nodules developed by the mutants were
348 smaller and paler, respect to Gifu (Figure 5B-D). Similarly, both size and nodule
349 numbers were affected in *expA1*-1 and *expA1*-2 mutants inoculated with IRBG74
350 (Figure 5E-H).

351

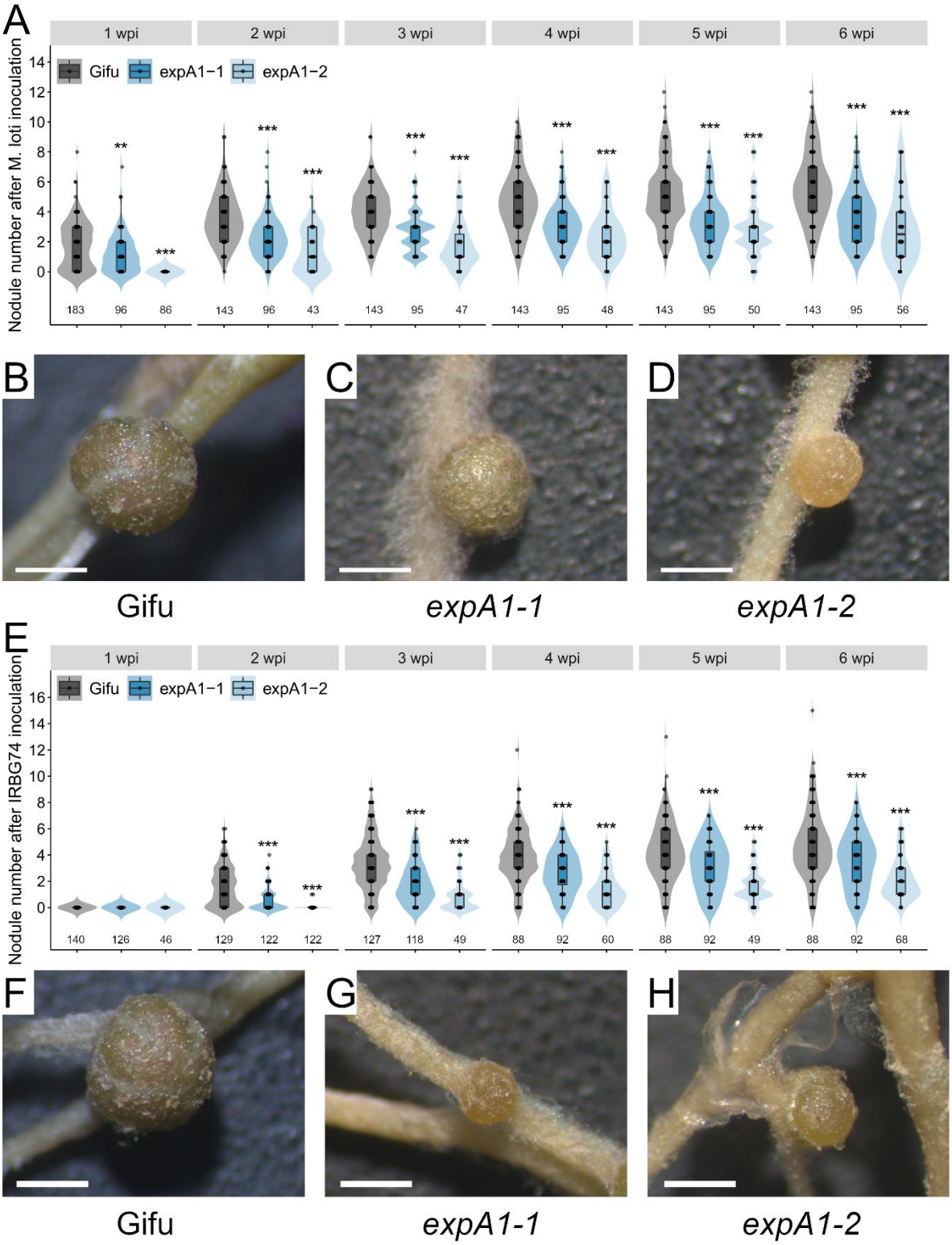

Figure 5. Compromised nodulation of *expA1* and *expA2* mutants after inoculation with *M. loti* R7A and IRBG74. Total number of nodules in Gifu (n=20), e*xpA1-1* (n=20) and e*xpA1-2* (n=20) at 1-6 wpi with *M. loti* **(A)** and IRBG74 **(E)**. Representative images of 3

356 weeks old nodules formed in Gifu **(B and F)**, *expA1-1* **(C and G)** and *expA1-2* **(D and H)** at
357 6 wpi with *M. loti* **(B-D)** and IRBG74 **(F-H)**. Scale 1 cm. In boxplots, the center line represents
358 means values of 3 independent experiments; box limits, upper and lower quartiles; whiskers,
359 1.5× interquartile range; points represent individual data points. The asterisk indicates
360 statistical significance between the *LORE1* mutant and Gifu according to Mann–Whitney U-
361 test (*$P < 0.05$; **$P < 0.01$; ***$P < 0.001$).

362

363 The collected evidence prompted us to monitor the two modalities of rhizobial
364 colonization in the two *expansin* mutants. In Gifu plants, the typical intracellular
365 infection through root hair ITs was observed at 7 dpi with *M. loti* R7A (Figure 6A). By
366 contrast, at this timepoint ITs were not observed in the *expA1*-1 and *expA1*-2
367 mutants, and rhizobia were rather found attached to the root hair tip or within
368 infection chambers (Figure 6B and C). Quantitative analysis of these observations
369 indicated that epidermal and cortical ITs *per* root were reduced by over 90 % in
370 *expA1*-1 and *expA1*-2 mutants compared to Gifu (Figure 6G). Subsequently, we
371 evaluated the intercellular colonization of *A. pusense* IRBG74 in the different
372 genotypes, following the approaches that we have established to assess the *Lotus*-
373 IRBG74 symbiosis (Montiel et al. 2021). In accordance with previous reports,
374 IRBG74 promotes the formation of infection pockets in swollen and twisted root hairs
375 at 7 dpi (Figure 6D). These responses also occurred in the *expA1*-1 and *expA1*-2
376 mutants inoculated with *A. pusense* IRBG74, but apparently with fewer and less
377 colonized infection pockets (Figure 6E and F). Based on these findings, we followed
378 a root endosphere protocol to evaluate by qPCR, the rhizobial *nodA* abundance in
379 genomic DNA samples isolated from roots of Gifu and the *Expansin* mutants at 3 wpi
380 with IRBG74. The presence of the IRBG74-*nodA* gene was 64-87% lower in the
381 *expA1*-1, and *expA1*-2 mutants compared to Gifu, reflecting a compromised
382 intercellular colonization of the roots by IRBG74 (Figure 6H).

383

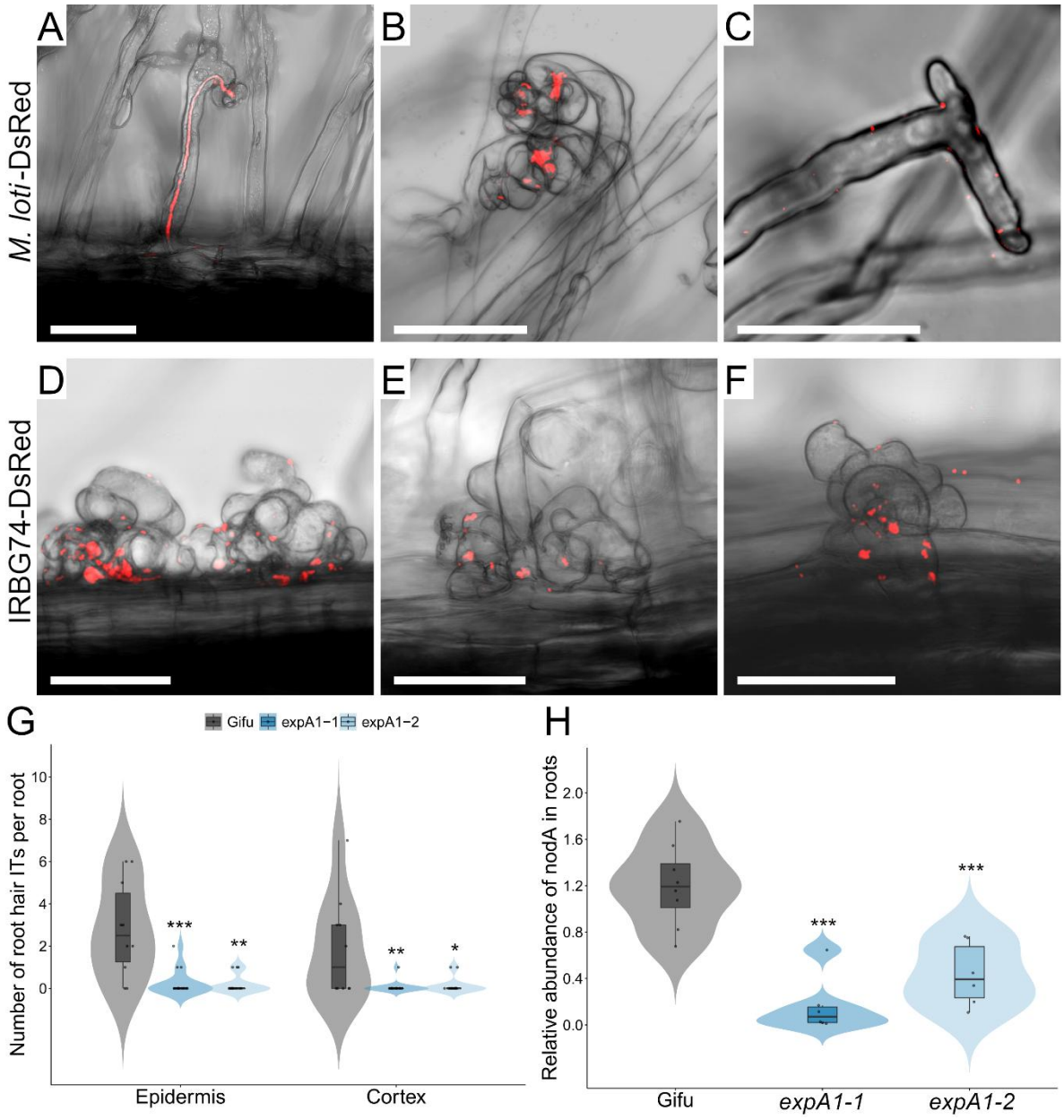

Figure 6. Altered rhizobial infection in *expA1* mutants. Confocal microscopy images of rhizobial colonization in Gifu (**A** and **D**), *expA1*-1 (**B** and **E**) and *expA1*-2 (**C** and **F**) roots at 7 dpi with *M. loti*-DsRed (**A**-**C**) and IRBG74-DsRed (**D**-**F**). **G**, Number of root hair ITs found in the epidermis and cortex at 10 dpi with *M. loti*–DsRed on Gifu (n = 10), *expA1*-1 (n = 15) and *expA1*-2 (n = 15). **H**, Abundance of IRBG74-*nodA* by qPCR in genomic DNA isolated from Gifu (n = 8), *expA1*-1 (n = 6) and *expA1*-2 (n = 6) at 3 wpi with IRBG74 and normalized to the *LjNFR5* gene accumulation.

393 **Discussion**

394

395 **Differential expression of *Lotus* Expansins in biotic interactions**

396 Over recent decades, a range of studies have documented that Expansins form a
397 multigene family in plants, mostly composed by four subfamilies (Cosgrove, 2024,
398 Wang *et al.*, 2024). The selected species in our phylogenetic analysis show a higher
399 abundance of the alpha subfamily with an increased representation of the EXLB
400 group in legumes relative to non-legumes, an observation that is consistent with
401 other studies (Guimaraes *et al.*, 2017, Wang *et al.*, 2024). While the alpha and beta
402 subfamilies are extensively documented in the literature for loosening the plant cell
403 wall during developmental programs and in response to (a)biotic stimuli, reports on
404 the roles of EXLA and EXLB members remain limited (Cosgrove, 2015). When
405 analyzing the transcriptomic profile of *Lotus* Expansins in response to biotic
406 interactions, we found that most of the *EXLBs* increase their expression after
407 inoculation with the pathogens *Pseudomonas syringae* and *Ralstonia solanacearum*
408 (Kelly *et al.*, 2018). Different studies conducted in *Arachis* spp., confirm the relevant
409 role of *EXLB* in response to pathogen perception, since the heterologous ectopic
410 expression of *Arachis duranensis EXLB8* confers resistance towards *Sclerotinia*
411 *sclerotiorum* and *Meloidogyne incognita* attack (Guimaraes *et al.*, 2017, Brasileiro *et*
412 *al.*, 2021). Herein, we observed that expression of one *EXLB* gene
413 (LotjaGi4g1v0195900) was significantly induced at 1 dpi with *M. loti*. The analysis of
414 the expression data in *Lotus* also revealed that during arbuscular mycorrhiza
415 symbiosis (AMS), Expansins of the four subfamilies are notably upregulated. In
416 contrast, only a small subset of Expansins exhibit high expression levels in nodules
417 or at initial stages of intra/intercellular rhizobial colonization. Among these,
418 LotjaGi1g1v606600, which encodes an EXPB isoform, is the potential ortholog of
419 soybean EXPB1, based on its phylogenetic distribution. *GmEXPB1* promoter is
420 strongly expressed in different tissues of developing soybean nodules, and
421 transgenic plants with altered transcript levels of *GmEXPB1* by RNAi or
422 overexpression, are affected in nodule size and number (Li *et al.*, 2015).

423

424 Likewise, the involvement of alpha Expansins in various biotic interactions has been
425 documented. In *Nicotiana benthamiana* leaves, Turnip mosaic virus (TuMV) leads
426 to a downregulation of both transcript and protein levels of the plasmodesmata-
427 specific EXPA1. Furthermore, overexpression of *NbEXPA1* increases resistance to
428 TuMV infection, while its silencing decreases it (Park *et al.*, 2017). Conversely, in
429 *Nicotiana tabacum*, overexpression of the alpha Expansin *EXPA4* promotes disease
430 progression caused by *Pseudomonas syringae* DC3000 (Chen *et al.*, 2018). While
431 several studies show that at different stages of the legume-rhizobia symbiosis
432 different *Expansins* are transcriptionally induced (Gyorgyey *et al.*, 2000, Giordano
433 and Hirsch, 2004, Libourel *et al.*, 2023), their specific functional roles remain scarcely
434 characterized. In *Lotus*, six alpha Expansins were significantly upregulated at 1-3
435 dpi with *M. loti*, whereas only four members of this subfamily were induced by
436 IRBG74 at 3-10 dpi. Notably, the expression of 2 alpha Expansins was repressed in
437 response to *M. loti*, and one after IRBG74 inoculation, suggesting that certain
438 Expansins might play a negative role during rhizobial infection.

439

440 **Cell wall rearrangement during rhizobial colonization and nodule development**
441 Prior to the formation of the IT, the microsymbiont attaches to the apical region of
442 the root hair, leading to swelling and curling of the root hair, that traps the rhizobia
443 within an infection chamber. This process requires significant cellular changes, as
444 the apical growth of the root hair cell wall is reversed (Fournier *et al.*, 2008, Gao *et*
445 *al.*, 2024). Recent evidence revealed that Glycoside Hydrolase 9C2, a cell wall
446 degrading enzyme, is abundantly accumulated in the infection chamber (IC) of *M.*
447 *truncatula* root hairs. In addition, mutant lines disrupted in *GH9C2* display aberrant
448 ITs (Zhao *et al.*, 2025). Similarly, abnormal IC are formed in the *nodulation pectate*
449 *lyase* (*npl*) mutant in *L. japonicus* (Xie *et al.*, 2012). These studies reveal that
450 enzymatic degradation of cell wall components in root hairs, mediated by GH9C and
451 NPL, is essential for intracellular rhizobial infection. Our study presents evidence
452 that also EXPA1 contributes significantly to intracellular symbiotic colonization in *L.*
453 *japonicus*. EXPA1 was prominently localized within the IC, and mutants deficient in
454 *EXPA1* showed marked defects in IT development. Importantly, EXPA1 strongly

455 accumulated at the so-called transcellular passage cleft (Zhang and Ott, 2024). This
456 localization pattern correlates with the cytolocalization of NPL and symbiosis-specific
457 pectin methyl esterase (SyPME1) in *M. truncatula*, where the coordinated action of
458 both proteins is essential to alter the IT cell wall biomechanics during the transcellular
459 invasion of rhizobia (Su *et al.*, 2023). Our results show that, in addition to the
460 enzymatic activity of cell wall remodeling proteins, the non-catalytic cell wall
461 relaxation mediated by EXPA1, occurs at critical stages of intracellular rhizobial
462 infection.
463 The molecular mechanisms underlying intercellular colonization in legume-rhizobia
464 symbiosis remain largely unclear, even though this process occurs in roughly 25%
465 of nodulating legume genera (Sprent 2007). In this regard, we recently reported that
466 *A. pusense* IRBG74 infects *Lotus* roots intercellularly, establishing it as a novel
467 working model to study this process (Montiel *et al.*, 2021). Notably, both the total
468 number of nodules and the number of pink nodules is comparable in plants
469 inoculated with either IRBG74 or the cognate rhizobial strain *M. loti*. In contrast, the
470 *Ljnlp* mutant exhibits a more pronounced reduction in nodule formation within the
471 *Lotus*-IRBG74 symbiosis than in the *Lotus-M. loti* association (Montiel et al. 2021),
472 indicating a greater impact on the intercellular infection mechanism by the loss of
473 function in the symbiotic pectate lyase. An initial response observed during the
474 intercellular colonization of IRBG74 in *Lotus* roots is extensive curling and twisting
475 of root hairs. This event is subsequently followed by the formation of infection
476 pockets (IP) within the root hairs; from these IP, the bacteria migrate intercellularly
477 toward a deeper layer of the root tissue (Montiel *et al.*, 2021, Quilbe *et al.*, 2022). At
478 these steps of intercellular infection, EXPA1 was particularly abundant at the
479 periphery of swollen root hairs and IP, suggesting that cell wall remodeling by EXPA1
480 takes place in these processes.

481 EXPA1 was prominently expressed in dividing cortical cells during nodule primordia
482 development in plants with either intercellular or intracellular colonization.
483 Furthermore, the reduction in nodule formation observed in *expA1* mutants was
484 comparable when inoculated with either *M. loti* or IRBG74. While intracellular and
485 intercellular infections involve distinct transcriptomic and cellular pathways, a set of

genes is fundamental for both processes (Garcia-Soto *et al.*, 2023, Montiel *et al.*, 2023). Our findings indicate that *EXPA1* represents one such gene.

In summary, structural remodeling of the cell wall matrix at confined cellular domains in legume roots is crucial for rhizobial colonization, with different cell wall remodeling proteins being synergistically involved at multiple steps. Recent research has provided substantial insight into the intricate interplay among these components, but the picture is far from being complete. In this frame, the additional identification of members belonging to other well-known cell wall remodeling protein families such as the Expansins and the characterization of their role during symbiotic infection constitute a relevant contribution to the field.

Figure legends

Figure 1. Expression profile and phylogeny of *Lotus* Expansins. **A,** Heat map expression of *Lotus* genes encoding Expansins in roots inoculated with *M. loti* and IRBG74 (extracted from RNAseq data; Montiel et al. 2021). **B,** Expression pattern of *LjExpA1* (LotjaGi1g1v0089200) extracted from single-cell RNAseq data (Frank et al. 2023). **C,** Phylogenetic distribution of *Lotus* Expansins across four subfamilies: alpha, beta, alpha-like, and beta-like.

Figure 2. Promoter activity of *LjEXPA1* during intercellular and intracellular rhizobial infection. Confocal microscopy images of *Lotus* transgenic roots expressing the *pLjEXPA1*::*tYFP*-nls construct in uninoculated plants (**A-C**), and after inoculation with *M. loti*-DsRed **(D and E)** and IRBG74-DsRed **(F and H)**. IT, infection thread; IP, infection pocket.

Figure 3. Subcellular localization of LjEXPA1 during intracellular rhizobial infection. Live-cell confocal images of Lotus transgenic roots expressing the *pEXPA1::EXPA1-YFP_p35S::DsRed-nls* construct at different stages of *M. loti* colonization: **A,** Infection chamber (IC) formation; **B,** Infection thread (IT) progression; **C,** Transcellular passage cleft (TPC). Images are maximum intensity projections of z-stacks (step size = 1 µm) showing either the merge of the YFP (green) and DsRed (magenta) channels with (left) or without (middle) the bright field (BF) channel, or the isolated YFP channel (green fire blue, right). At least twelve composite plants from two independent experiments were analyzed. IC = infection chamber; IT = infection thread; TPC = transcellular passage cleft. Scale = 10 µm.

Figure 4. Subcellular localization of LjEXPA1 during intercellular infection. Live-cell confocal images of *Lotus* transgenic roots expressing the *pEXPA1::EXPA1-YFP_p35S::tDsRed-nls* construct at different steps of intercellular colonization by *A. pusense* IRBG74-DsRed: **A** and **C**, Root hairs swelling and twisting; **B** and **C**, Infection pocket formation (IP). Images are maximum intensity projections of z-stacks (step size = 1 µm) showing the merge of the YFP (green) and DsRed (magenta) channels with (left) or without (right) the bright field (BF) channel. At least twelve composite plants from two independent experiments were analyzed. IC = infection chamber; IT = infection thread; TPC = transcellular passage cleft. Scale = 10 µm.

530

531 **Figure 5. Compromised nodulation of *expA1* and *expA2* mutants after inoculation with**
532 ***M. loti* R7A and IRBG74.** Total number of nodules in Gifu (n=20), e*xpA1-1* (n=20) and
533 e*xpA1-2* (n=20) at 1-6 wpi with *M. loti* **(A)** and IRBG74 **(E)**. Representative images of 3
534 weeks old nodules formed in Gifu **(B and F)**, *expA1-1* **(C and G)** and *expA1-2* **(D and H)** at
535 6 wpi with *M. loti* **(B-D)** and IRBG74 **(F-H)**. Scale 1 cm. In boxplots, the center line represents
536 means values of 3 independent experiments; box limits, upper and lower quartiles; whiskers,
537 1.5× interquartile range; points represent individual data points. The asterisk indicates
538 statistical significance between the *LORE1* mutant and Gifu according to Mann–Whitney U-
539 test (**P* < 0.05; ***P* < 0.01; ****P* < 0.001).

540

541 **Figure 6. Altered rhizobial infection in *expA1* mutants.** Confocal microscopy images of
542 rhizobial colonization in Gifu (**A** and **D**), *expA1*-1 (**B** and **E**) and *expA1*-2 (**C** and **F**) roots at
543 7 dpi with *M. loti*-DsRed (**A**-**C**) and IRBG74-DsRed (**D**-**F**). **G**, Number of root hair ITs found
544 in the epidermis and cortex at 10 dpi with *M. loti*–DsRed on Gifu (n = 10), *expA1*-1 (n = 15)
545 and *expA1*-2 (n = 15). **H**, Abundance of IRBG74-*nodA* by qPCR in genomic DNA isolated
546 from Gifu (n = 8), *expA1*-1 (n = 6) and *expA1*-2 (n = 6) at 3 wpi with IRBG74 and normalized
547 to the *LjNFR5* gene accumulation.

548

549 **Supplementary information**

550

551 **Figure S1. Variable expression pattern of *Lotus Expansins* in different organs and**
552 **tissues.** Heat map gene expression of *Lotus Expansins* in aerial and ground tissues/organs,
553 under non-symbiotic, symbiotic and pathogenic conditions. Data collected from *Lotus* base
554 (https://lotus.au.dk/). AMS, arbuscular mycorrhiza symbiosis; RNS, root nodule symbiosis.

555

556 **Figure S2. Phylogeny and composition of the Expansin family in different plant**
557 **species**. Phylogenetic distribution **(A)** and number **(B)** of alpha, beta, alpha-like and beta-
558 like Expansins in *Physcomitrella patens, A. thaliana, Oryza sativa, Glycine soja, Phaseolus*
559 *vulgaris, Medicago truncatula* and *L. japonicus*. EXPA1 is highlighted with an arrow.
560 LotjaGi1g1v060600, marked with an asterisk, is the putative orthologue of GmEXPB2 (Li et

561 al. 2015). **C)** Identity matrix of *Lotus* Expansins represented by heatmap using the predicted
562 amino acid sequences. Made on Uniprot (https://www.uniprot.org/align/).

563

564 **Figure S3. Subcellular localization of LjEXPA1 during nodule primordia formation.**
565 Live-cell confocal images of *Lotus* transgenic roots expressing the *pEXPA1::EXPA1-*
566 *YFP_p35S::tDsRed-nls* construct during nodule primordia formation after *M. loti* R7A-
567 DsRed **(A)** and IRBG74-DsRed colonization **(B)**. Images are single focal planes **(A)** or
568 maximum intensity projections of z-stacks (**B**, step size = 1 µm) showing either the merge
569 of the YFP (green) and DsRed (magenta) channels with (left) or without (middle) the bright
570 field (BF) channel, or the isolated YFP channel (green fire blue, right). At least twelve
571 composite plants from two independent experiments were analysed. Scale = 50 µm.

572

573 **Figure S4. Impact on transcript levels of *LjEXPA1* by *LORE1* insertions. A,** Schematic
574 representation of *LjEXPA1* gene disrupted by LORE1 insertions. Black boxes: exons;
575 Dashed lines, UTRs; Solid lines, introns. Retrotransposon insertions are indicated with red
576 triangles. **B,** Boxplots represent the normalized expression levels of *EXPA1,* calculated by
577 RT-qPCR from 4 independent biological replicates (n = 5 per biological replicate) in Gifu,
578 *expa1*-1 and *expA1*-2 roots.

579

580 **Funding information**

581 [1]This work was supported by the grant Engineering the Nitrogen Symbiosis for Africa made
582 to the University of Cambridge by the Bill & Melinda Gates Foundation (ENSA;
583 OPP11772165), the European Research Council (ERC) under the European Union's
584 Horizon 2020 research and innovation programme (grant agreement no. 834221), the
585 Mexican Secretaría de Ciencia, Humanidades, Tecnología e Innovación (SECIHTI, grant
586 CBF2023-2024-834 to J. M.) and Dirección General de Asuntos del Personal Académico
587 (DGAPA)-Universidad Nacional Autónoma de México (UNAM) – Programa de Apoyo a
588 Proyectos de Investigación e Innovación Tecnológica (PAPIIT, grant IA200723 and
589 IA200125 to J. M.). The work was additionally supported by the grants 403222702 (SFB
590 1381) and 414136422 of the German Research Association (Deutsche
591 Forschungsgemeinschaft) to T.O. The Leica SP8 FALCON FLIM microscope is operated by
592 the Microscopy and Image Analysis Platform (MIAP) and the Life Imaging Center (LIC),
593 Freiburg.

Author contributions

J.M. and J.S. planned and designed the research. J.M., I.G.S, B.L., E.M.M., N.S. and M.V., performed experiments. J.M., B.L., T.O. and J.S. revised the manuscript and provided resources and infrastructure. J.M. and E.M.M. wrote the manuscript.

Acknowledgements

We thank Mariana Robledo Gamboa for identifying the Expansin sequences in different plant species.

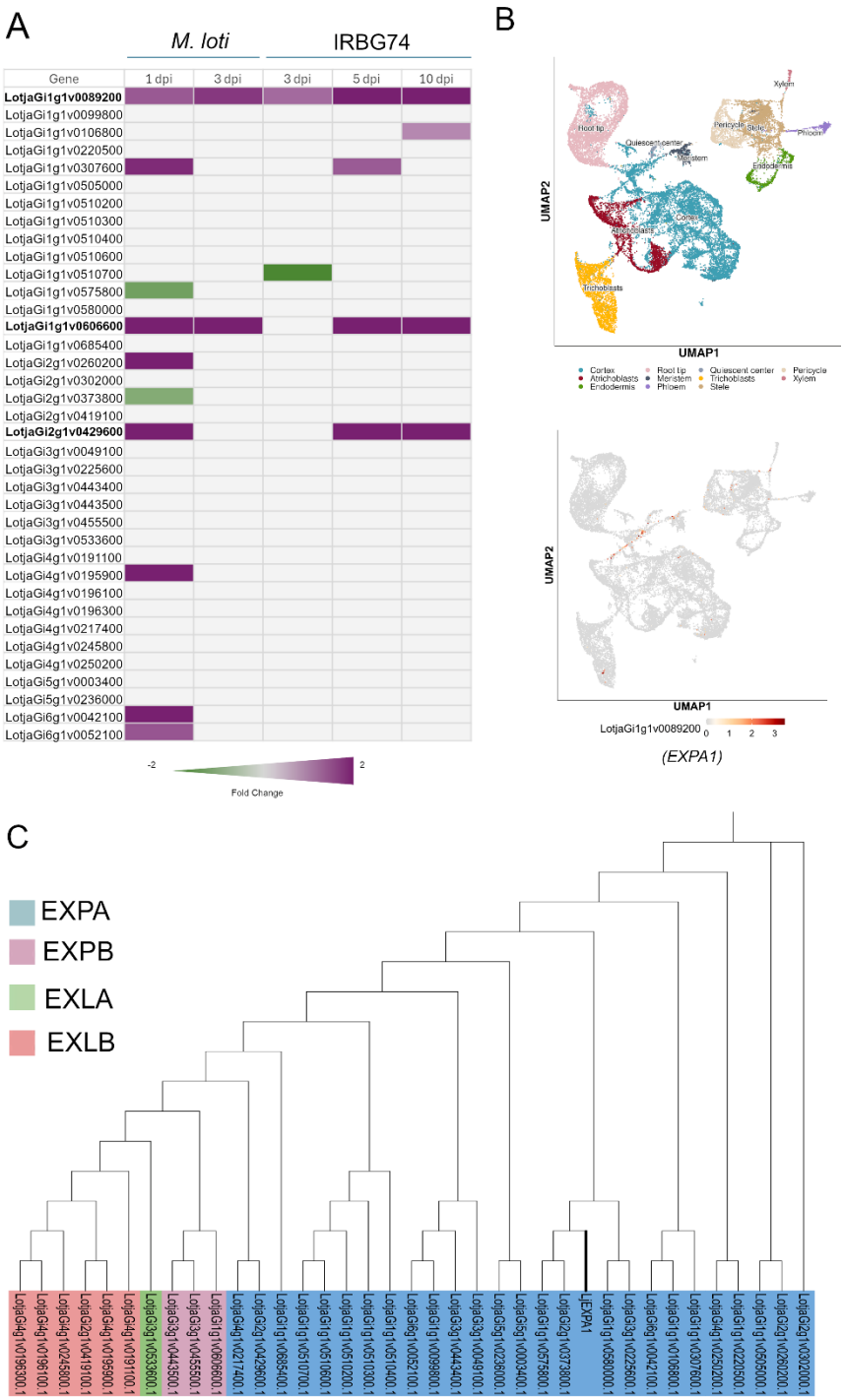

Figure 1. Expression profile and phylogeny of *Lotus* Expansins. **A,** Heat map expression of *Lotus* genes encoding Expansins in roots inoculated with *M. loti* and IRBG74 (extracted from RNAseq data; Montiel et al. 2021). **B,** Expression pattern of *LjExpA1* (LotjaGi1g1v0089200) extracted from single-cell RNAseq data (Frank et al. 2023). **C,** Phylogenetic distribution of *Lotus* Expansins across four subfamilies: alpha, beta, alpha-like, and beta-like.

613

614

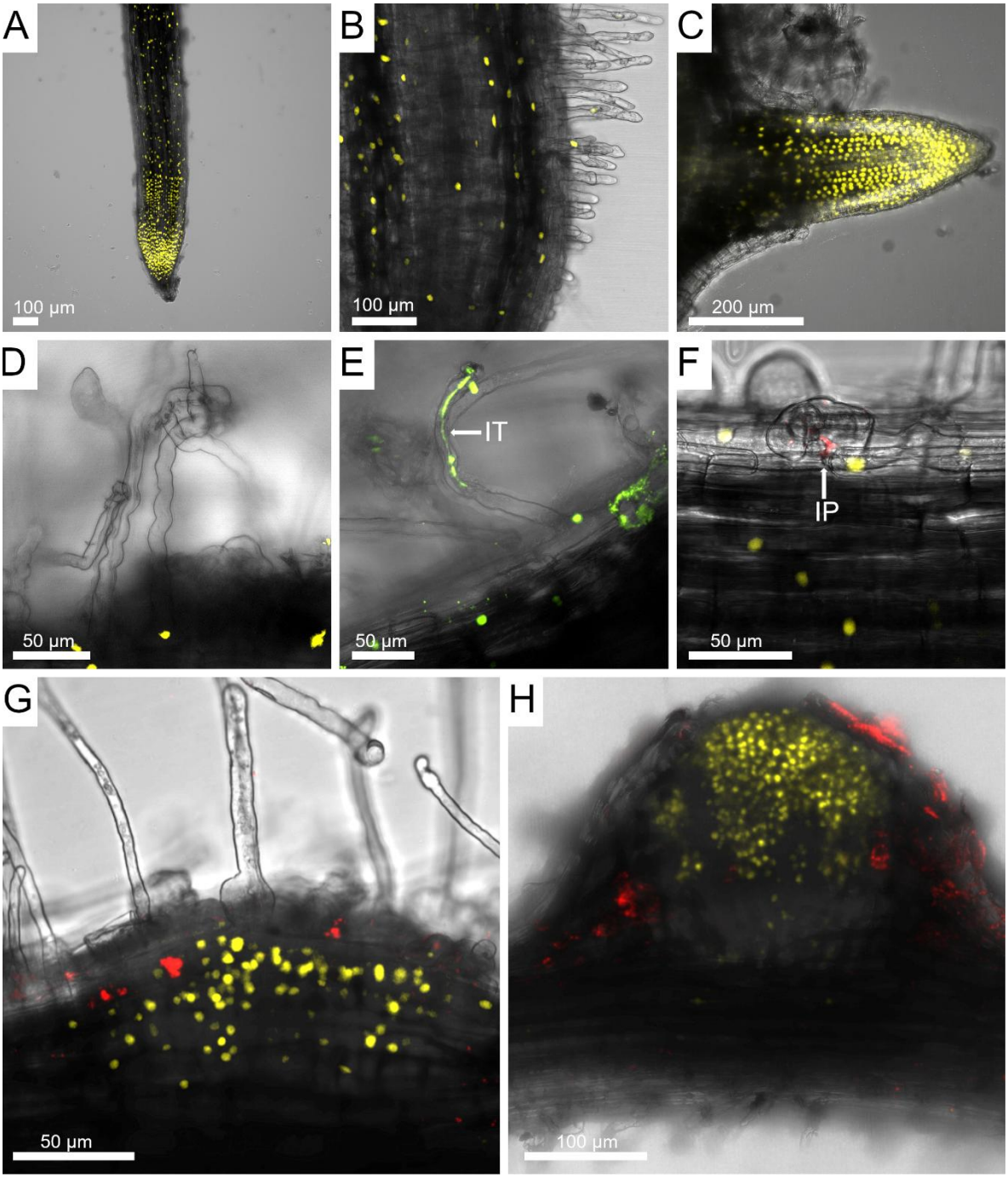

615

616 **Figure 2. Promoter activity of *LjEXPA1* during intercellular and intracellular rhizobial**
617 **infection.** Confocal microscopy images of *Lotus* transgenic roots expressing the
618 *pLjEXPA1*::*tYFP*-nls construct in uninoculated plants (**A-C**), and after inoculation with *M. loti*-
619 GFP **(D and E)** and IRBG74-DsRed **(F and H)**. IT, infection thread; IP, infection pocket.

620

621

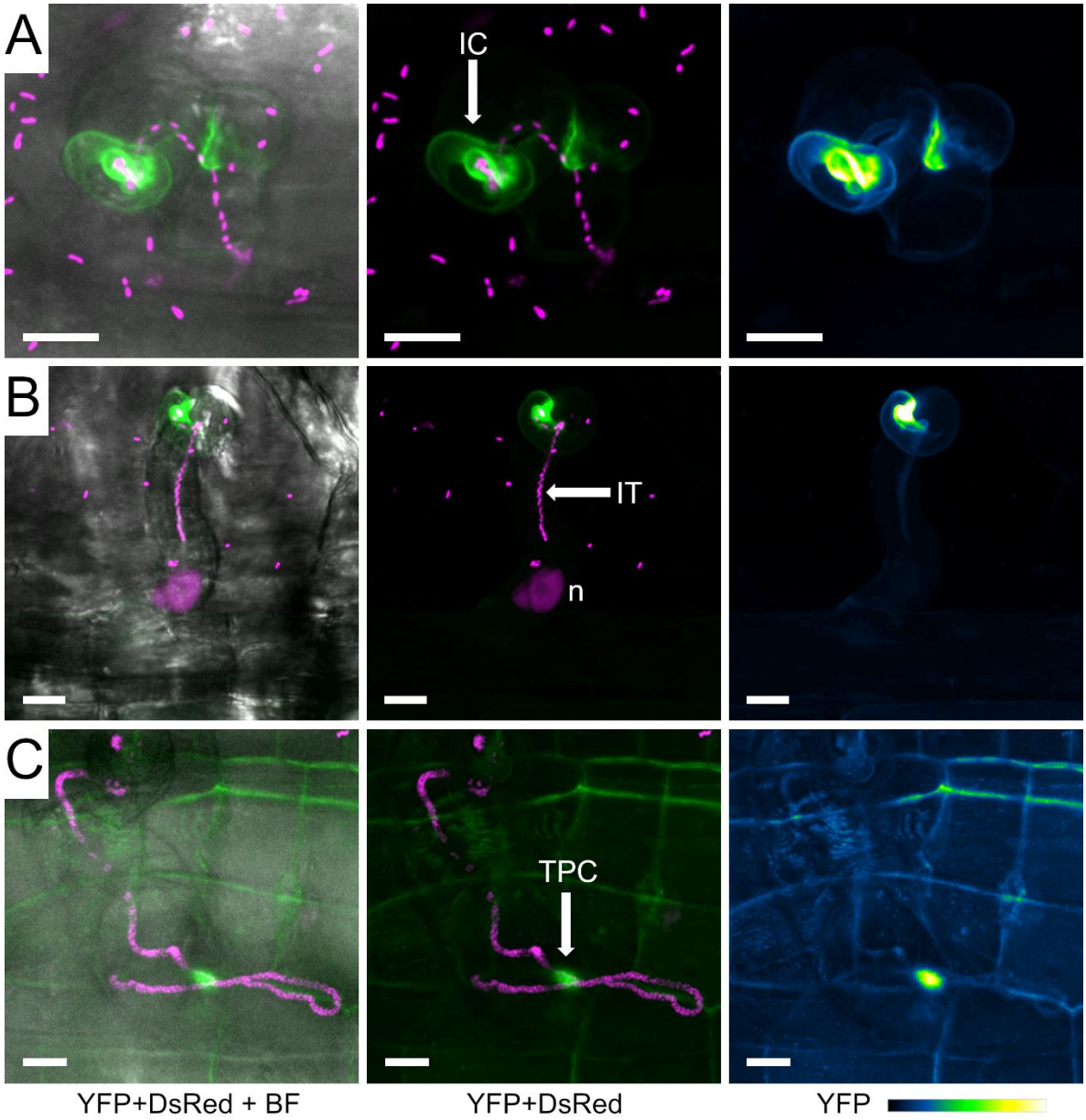

622

623 **Figure 3. Subcellular localization of LjEXPA1 during intracellular rhizobial infection.**
624 Live-cell confocal images of *Lotus* transgenic roots expressing the *pEXPA1::EXPA1-*
625 *YFP_p35S::DsRed-nls* construct at different stages of *M. loti* colonization: **A,** Infection
626 chamber (IC) formation; **B,** Infection thread (IT) progression; **C,** Transcellular passage cleft
627 (TPC). Images are maximum intensity projections of z-stacks (step size = 1 µm) showing
628 either the merge of the YFP (green) and DsRed (magenta) channels with (left) or without
629 (middle) the bright field (BF) channel, or the isolated YFP channel (green fire blue, right). At
630 least twelve composite plants from two independent experiments were analyzed. IC =
631 infection chamber; IT = infection thread; TPC = transcellular passage cleft. Scale = 10 µm.

632

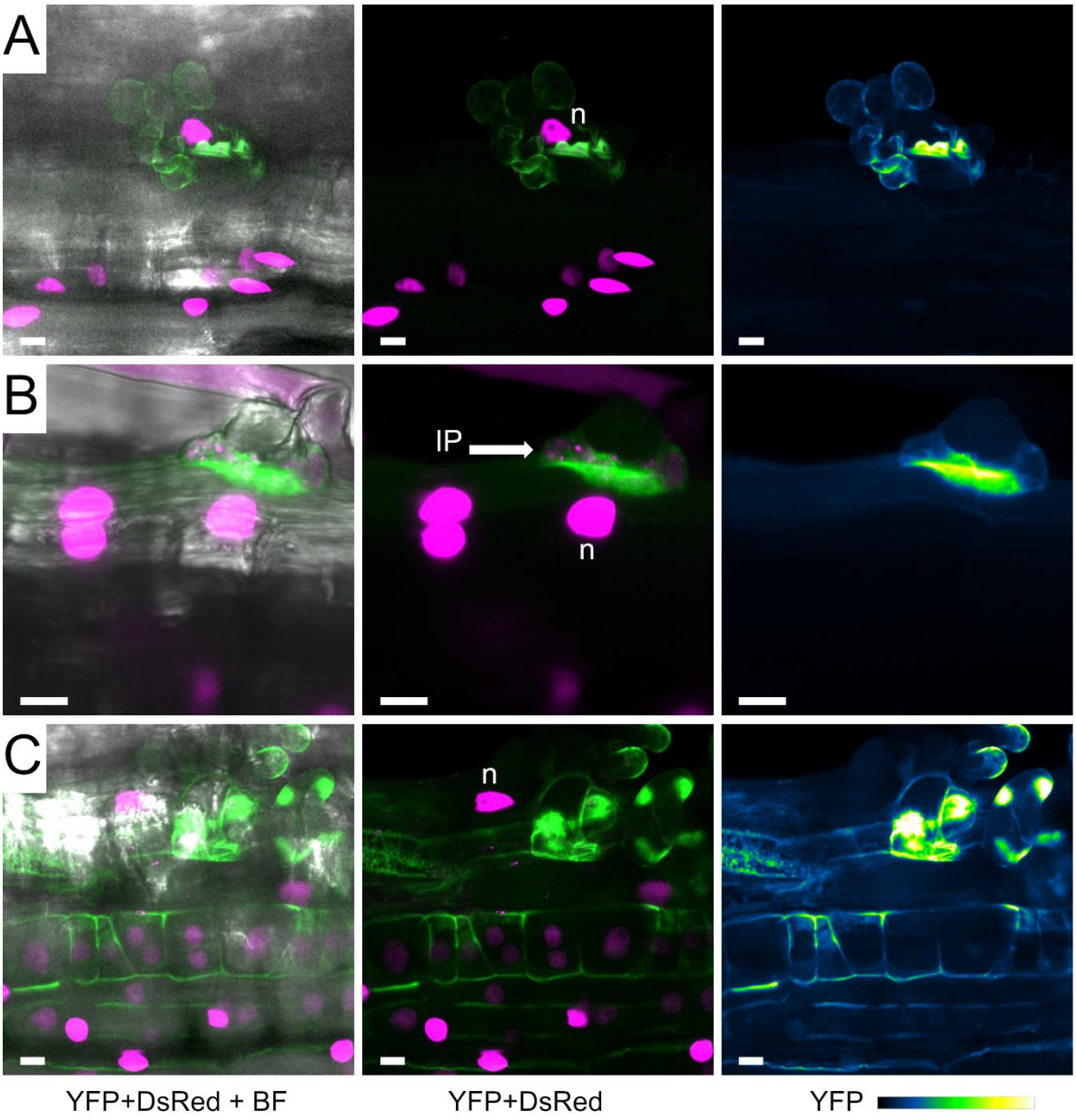

Figure 4. Subcellular localization of LjEXPA1 during intercellular infection. Live-cell confocal images of *Lotus* transgenic roots expressing the *pEXPA1::EXPA1-YFP_p35S::tDsRed-nls* construct at different steps of intercellular colonization by *A. pusense* IRBG74-DsRed: **A**, Root hairs swelling and twisting; **B**, Infection pocket formation (IP); **C**, Cortical cell division. Images are maximum intensity projections of z-stacks (step size = 1 µm) showing either the merge of the YFP (green) and DsRed (magenta) channels with (left) or without (middle) the bright field (BF) channel, or the isolated YFP channel (green fire blue, right). At least twelve composite plants from two independent experiments were analyzed. IC = infection chamber; IT = infection thread; TPC = transcellular passage cleft. Scale = 10 µm.

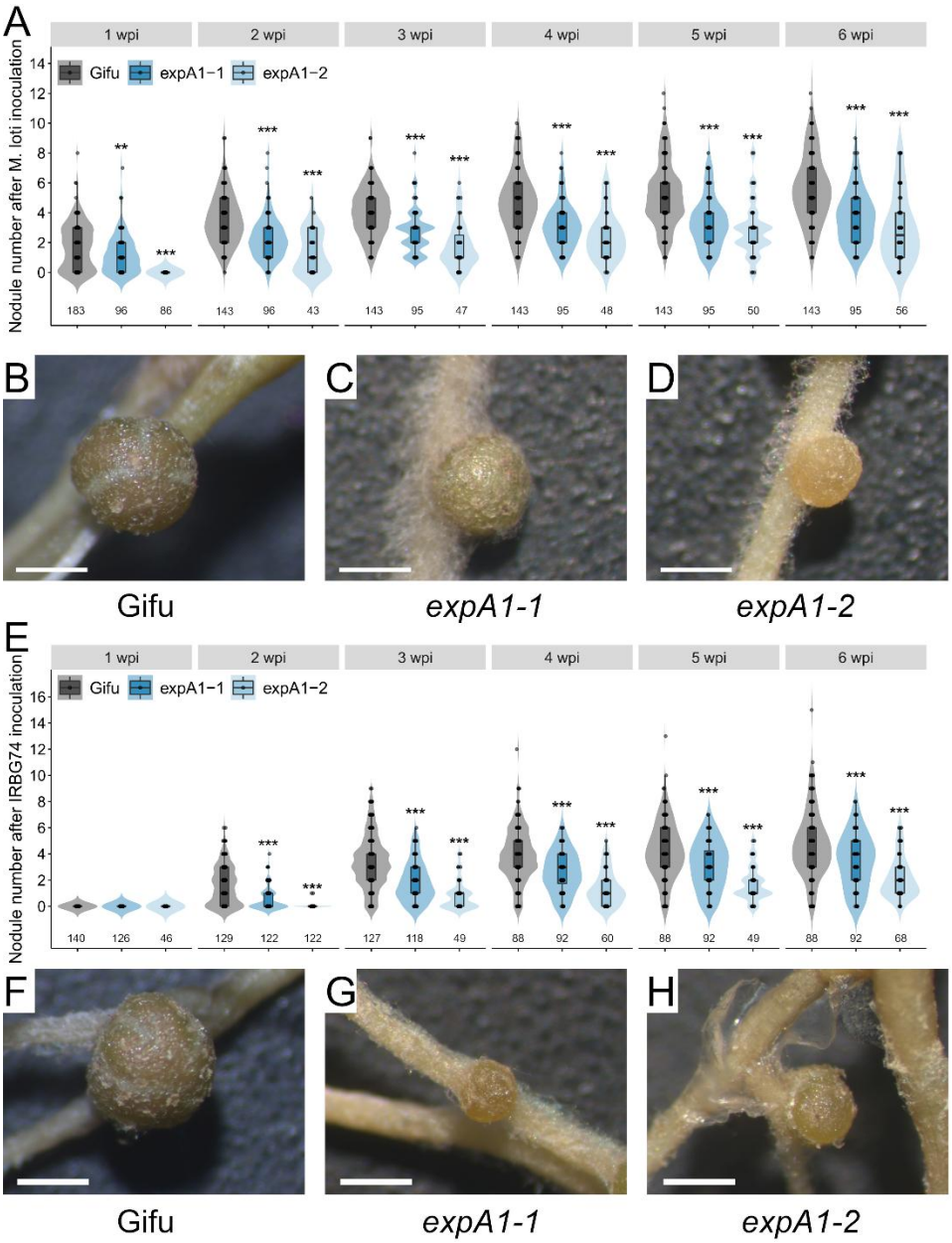

Figure 5. Compromised nodulation of *expA1* and *expA2* mutants after inoculation with *M. loti* R7A and IRBG74. Total number of nodules in Gifu (n > 50), e*xpA1-1* (n > 50) and e*xpA1-2* (n > 50) at 1-6 wpi with *M. loti* **(A)** and IRBG74 **(E)**. Representative images of 3 weeks old nodules formed in Gifu **(B and F)**, *expA1-1* **(C and G)** and *expA1-2* **(D and H)** at 6 wpi with *M. loti* **(B-D)** and IRBG74 **(F-H)**. Scale 1 cm. In boxplots, the center line represents means values of independent experiments; box limits, upper and lower quartiles; whiskers, 1.5× interquartile range; points represent individual data points. The asterisk indicates statistical significance between the *LORE1* mutant and Gifu according to Mann–Whitney U-test (**P* < 0.05; ***P* < 0.01; ****P* < 0.001). Below the violin plots the number of plants is indicated.

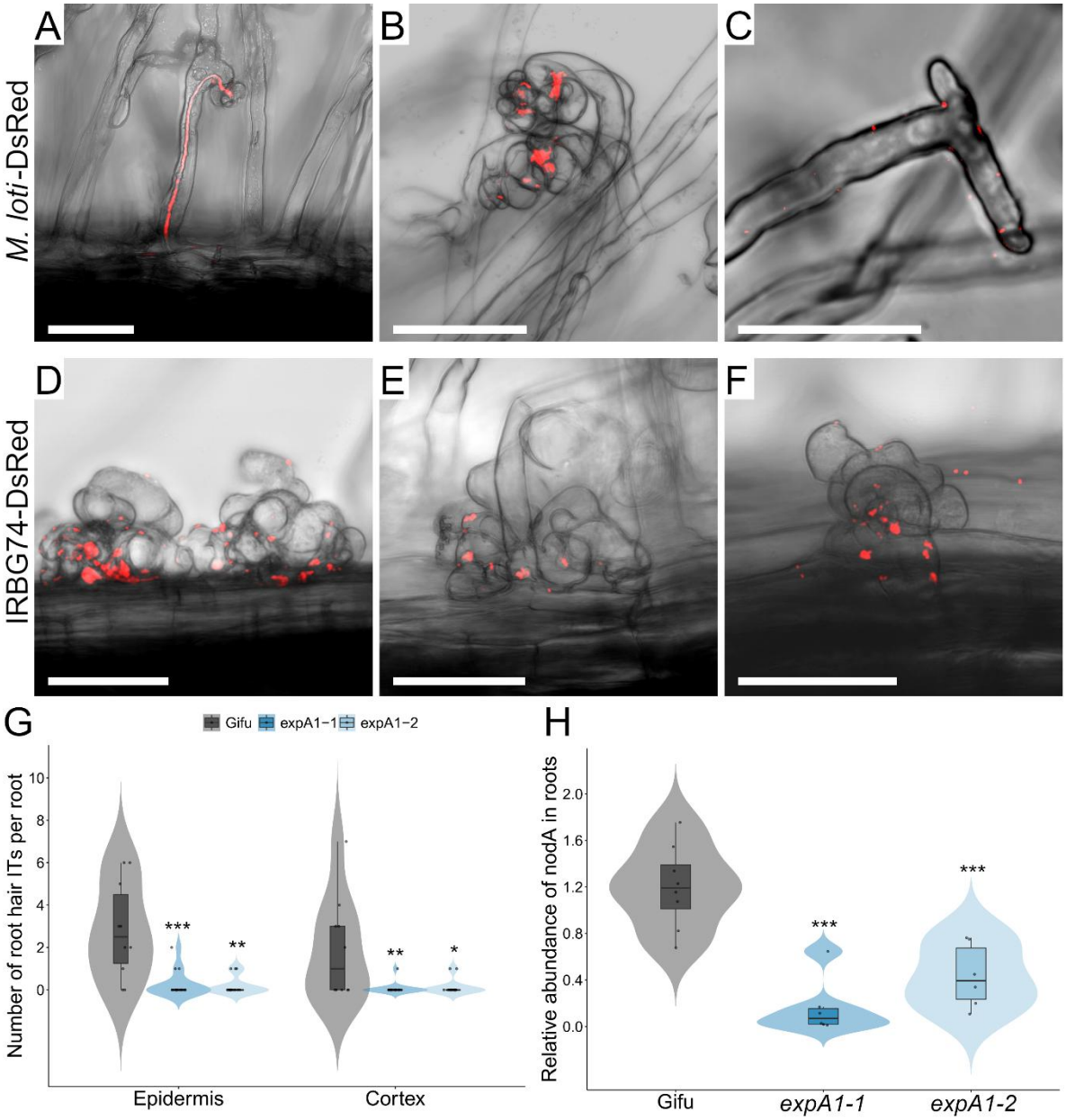

Figure 6. Altered rhizobial infection in *expA1* mutants. Confocal microscopy images of rhizobial colonization in Gifu (**A** and **D**), *expA1*-1 (**B** and **E**) and *expA1*-2 (**C** and **F**) roots at 7 dpi with *M. loti*-DsRed (**A**-**C**) and IRBG74-DsRed (**D**-**F**). **G**, Number of root hair ITs found in the epidermis and cortex at 10 dpi with *M. loti*–DsRed on Gifu (n = 10), *expA1*-1 (n = 15) and *expA1*-2 (n = 15). **H**, Abundance of IRBG74-*nodA* by qPCR in genomic DNA isolated from Gifu (n = 8), *expA1*-1 (n = 6) and *expA1*-2 (n = 6) at 3 wpi with IRBG74 and normalized to the *LjNFR5* gene accumulation.

667

668 ## Bibliography

669

670 **Acosta-Jurado, S., Rodriguez-Navarro, D.N., Kawaharada, Y., Perea, J.F., Gil-Serrano, A., Jin, H., An,**
671 **Q., Rodriguez-Carvajal, M.A., Andersen, S.U., Sandal, N., Stougaard, J., Vinardell, J.M. and**
672 **Ruiz-Sainz, J.E.** (2016) Sinorhizobium fredii HH103 Invades Lotus burttii by Crack Entry in a
673 Nod Factor-and Surface Polysaccharide-Dependent Manner. *Mol Plant Microbe Interact*, **29**,
674 925-937.
675 **Bozsoki, Z., Gysel, K., Hansen, S.B., Lironi, D., Kronauer, C., Feng, F., de Jong, N., Vinther, M.,**
676 **Kamble, M., Thygesen, M.B., Engholm, E., Kofoed, C., Fort, S., Sullivan, J.T., Ronson, C.W.,**
677 **Jensen, K.J., Blaise, M., Oldroyd, G., Stougaard, J., Andersen, K.R. and Radutoiu, S.** (2020)
678 Ligand-recognizing motifs in plant LysM receptors are major determinants of specificity.
679 *Science*, **369**, 663-670.
680 **Brasileiro, A.C.M., Lacorte, C., Pereira, B.M., Oliveira, T.N., Ferreira, D.S., Mota, A.P.Z., Saraiva,**
681 **M.A.P., Araujo, A.C.G., Silva, L.P. and Guimaraes, P.M.** (2021) Ectopic expression of an
682 expansin-like B gene from wild Arachis enhances tolerance to both abiotic and biotic
683 stresses. *Plant J*, **107**, 1681-1696.
684 **Broughton, W.J. and Dilworth, M.J.** (1971) Control of leghemoglobin synthesis in snake beans.
685 *Biochemical J.*, **125**, 1075-1080.
686 **Broxterman, S.E. and Schols, H.A.** (2018) Interactions between pectin and cellulose in primary plant
687 cell walls. *Carbohydr Polym*, **192**, 263-272.
688 **Chen, L.J., Zou, W.S., Fei, C.Y., Wu, G., Li, X.Y., Lin, H.H. and Xi, D.H.** (2018) alpha-Expansin EXPA4
689 Positively Regulates Abiotic Stress Tolerance but Negatively Regulates Pathogen Resistance
690 in Nicotiana tabacum. *Plant Cell Physiol*, **59**, 2317-2330.
691 **Cosgrove, D.J.** (2015) Plant expansins: diversity and interactions with plant cell walls. *Curr Opin Plant*
692 *Biol*, **25**, 162-172.
693 **Cosgrove, D.J.** (2024) Plant Cell Wall Loosening by Expansins. *Annu Rev Cell Dev Biol*, **40**, 329-352.
694 **de Carvalho-Niebel, F., Fournier, J., Becker, A. and Marin Arancibia, M.** (2024) Cellular insights into
695 legume root infection by rhizobia. *Curr Opin Plant Biol*, **81**, 102597.
696 **Downie, J.A.** (2014) Legume nodulation. *Curr Biol*, **24**, R184-190.
697 **Feng, X., Li, C., He, F., Xu, Y., Li, L., Wang, X., Chen, Q. and Li, F.** (2022) Genome-Wide Identification
698 of Expansin Genes in Wild Soybean (Glycine soja) and Functional Characterization of
699 Expansin B1 (GsEXPB1) in Soybean Hair Root. *Int J Mol Sci*, **23**.
700 **Ferguson, B.J., Indrasumunar, A., Hayashi, S., Lin, M.H., Lin, Y.H., Reid, D.E. and Gresshoff, P.M.**
701 (2010) Molecular analysis of legume nodule development and autoregulation. *J Integr Plant*
702 *Biol*, **52**, 61-76.
703 **Fournier, J., Timmers, A.C., Sieberer, B.J., Jauneau, A., Chabaud, M. and Barker, D.G.** (2008)
704 Mechanism of infection thread elongation in root hairs of Medicago truncatula and dynamic
705 interplay with associated rhizobial colonization. *Plant Physiol*, **148**, 1985-1995.
706 **Gao, J.P., Liang, W., Liu, C.W., Xie, F. and Murray, J.D.** (2024) Unraveling the rhizobial infection
707 thread. *J Exp Bot*, **75**, 2235-2245.
708 **Garcia-Soto, I., Andersen, S.U., Monroy-Morales, E., Robledo-Gamboa, M., Guadarrama, J., Aviles-**
709 **Baltazar, N.Y., Serrano, M., Stougaard, J. and Montiel, J.** (2023) A collection of novel Lotus
710 japonicus LORE1 mutants perturbed in the nodulation program induced by the
711 Agrobacterium pusense strain IRBG74. *Front Plant Sci*, **14**, 1326766.

712 **Giordano, W. and Hirsch, A.M.** (2004) The expression of MaEXP1, a Melilotus alba expansin gene, is
713 upregulated during the sweetclover-Sinorhizobium meliloti interaction. *Mol Plant Microbe*
714 *Interact*, **17**, 613-622.
715 **Guimaraes, L.A., Mota, A.P.Z., Araujo, A.C.G., de Alencar Figueiredo, L.F., Pereira, B.M., de Passos**
716 **Saraiva, M.A., Silva, R.B., Danchin, E.G.J., Guimaraes, P.M. and Brasileiro, A.C.M.** (2017)
717 Genome-wide analysis of expansin superfamily in wild Arachis discloses a stress-responsive
718 expansin-like B gene. *Plant Mol Biol*, **94**, 79-96.
719 **Gyorgyey, J., Vaubert, D., Jimenez-Zurdo, J.I., Charon, C., Troussard, L., Kondorosi, A. and**
720 **Kondorosi, E.** (2000) Analysis of Medicago truncatula nodule expressed sequence tags. *Mol*
721 *Plant Microbe Interact*, **13**, 62-71.
722 **Handberg, K. and Stougaard, J.** (1992) Lotus japonicus, an autogamous, diploid legume species for
723 classical and molecular genetics. *Plant J*, **2**, 487-496.
724 **Hansen, J., Jorgensen, J.E., Stougaard, J. and Marcker, K.A.** (1989) Hairy roots - a short cut to
725 transgenic root nodules. *Plant Cell Rep*, **8**, 12-15.
726 **Ibañez, F., Wall, L. and Fabra, A.** (2017) Starting points in plant-bacteria nitrogen-fixing symbioses:
727 intercellular invasion of the roots. *J Exp Bot*, **68**, 1905-1918.
728 **Kamal, N., Mun, T., Reid, D., Lin, J.S., Akyol, T.Y., Sandal, N., Asp, T., Hirakawa, H., Stougaard, J.,**
729 **Mayer, K.F.X., Sato, S. and Andersen, S.U.** (2020) Insights into the evolution of symbiosis
730 gene copy number and distribution from a chromosome-scale Lotus japonicus Gifu genome
731 sequence. *DNA Res*, **27**.
732 **Karas, B., Murray, J., Gorzelak, M., Smith, A., Sato, S., Tabata, S. and Szczyglowski, K.** (2005)
733 Invasion of Lotus japonicus root hairless 1 by Mesorhizobium loti involves the nodulation
734 factor-dependent induction of root hairs. *Plant Physiol*, **137**, 1331-1344.
735 **Karas, B.J., Ross, L., Novero, M., Amyot, L., Shrestha, A., Inada, S., Nakano, M., Sakai, T., Bonetta,**
736 **D., Sato, S., Murray, J.D., Bonfante, P. and Szczyglowski, K.** (2021) Intragenic
737 complementation at the Lotus japonicus CELLULOSE SYNTHASE-LIKE D1 locus rescues root
738 hair defects. *Plant Physiol*, **186**, 2037-2050.
739 **Kelly, S., Mun, T., Stougaard, J., Ben, C. and Andersen, S.U.** (2018) Distinct Lotus japonicus
740 Transcriptomic Responses to a Spectrum of Bacteria Ranging From Symbiotic to Pathogenic.
741 *Front Plant Sci*, **9**, 1218.
742 **Kelly, S.J., Muszynski, A., Kawaharada, Y., Hubber, A.M., Sullivan, J.T., Sandal, N., Carlson, R.W.,**
743 **Stougaard, J. and Ronson, C.W.** (2013) Conditional requirement for exopolysaccharide in the
744 Mesorhizobium-Lotus symbiosis. *Mol Plant Microbe Interact*, **26**, 319-329.
745 **Kok, B.O., Celik Altunoglu, Y., Oncul, A.B., Karaci, A. and Cengiz Baloglu, M.** (2023) Expansin gene
746 family database: A comprehensive bioinformatics resource for plant expansin multigene
747 family. *J Bioinform Comput Biol*, **21**, 2350015.
748 **Lace, B. and Ott, T.** (2018) Commonalities and Differences in Controlling Multipartite Intracellular
749 Infections of Legume Roots by Symbiotic Microbes. *Plant Cell Physiol*, **59**, 661-672.
750 **Larkin, M.A., Blackshields, G., Brown, N.P., Chenna, R., McGettigan, P.A., McWilliam, H., Valentin,**
751 **F., Wallace, I.M., Wilm, A., Lopez, R., Thompson, J.D., Gibson, T.J. and Higgins, D.G.** (2007)
752 Clustal W and Clustal X version 2.0. *Bioinformatics*, **23**, 2947-2948.
753 **Li, X.X., Zhao, J., Tan, Z.Y., Zeng, R.S. and Liao, H.** (2015) GmEXPB2, a Cell Wall beta-Expansin, Affects
754 Soybean Nodulation through Modifying Root Architecture and Promoting Nodule Formation
755 and Development. *Plant Physiol*, **169**, 2640-2653.
756 **Liang, J., Klingl, A., Lin, Y.Y., Boul, E., Thomas-Oates, J. and Marin, M.** (2019) A subcompatible
757 rhizobium strain reveals infection duality in Lotus. *J Exp Bot*, **70**, 1903-1913.
758 **Libourel, C., Keller, J., Brichet, L., Cazale, A.C., Carrere, S., Vernie, T., Couzigou, J.M., Callot, C.,**
759 **Dufau, I., Cauet, S., Marande, W., Bulach, T., Suin, A., Masson-Boivin, C., Remigi, P., Delaux,**

760 **P.M. and Capela, D.** (2023) Comparative phylotranscriptomics reveals ancestral and derived
761 root nodule symbiosis programmes. *Nat Plants*, **9**, 1067-1080.
762 **Madsen, L.H., Tirichine, L., Jurkiewicz, A., Sullivan, J.T., Heckmann, A.B., Bek, A.S., Ronson, C.W.,**
763 **James, E.K. and Stougaard, J.** (2010) The molecular network governing nodule
764 organogenesis and infection in the model legume Lotus japonicus. *Nat Commun*, **1**, 10.
765 **Malolepszy, A., Mun, T., Sandal, N., Gupta, V., Dubin, M., Urbanski, D., Shah, N., Bachmann, A.,**
766 **Fukai, E., Hirakawa, H., Tabata, S., Nadzieja, M., Markmann, K., Su, J., Umehara, Y., Soyano,**
767 **T., Miyahara, A., Sato, S., Hayashi, M., Stougaard, J. and Andersen, S.U.** (2016) The LORE1
768 insertion mutant resource. *Plant J*, **88**, 306-317.
769 **Monroy-Morales, E., Davila-Delgado, R., Ayala-Guzman, E., Gamboa-deBuen, A. and Sanchez-**
770 **Lopez, R.** (2022) Visualization of the Crossroads between a Nascent Infection Thread and the
771 First Cell Division Event in Phaseolus vulgaris Nodulation. *Int J Mol Sci*, **23**.
772 **Montiel, J., Garcia-Soto, I., James, E.K., Reid, D., Cardenas, L., Napsucialy-Mendivil, S., Ferguson,**
773 **S., Dubrovsky, J.G. and Stougaard, J.** (2023) Aromatic amino acid biosynthesis impacts root
774 hair development and symbiotic associations in Lotus japonicus. *Plant Physiol*, **193**, 1508-
775 1526.
776 **Montiel, J., Reid, D., Gronbaek, T.H., Benfeldt, C.M., James, E.K., Ott, T., Ditengou, F.A., Nadzieja,**
777 **M., Kelly, S. and Stougaard, J.** (2021) Distinct signaling routes mediate intercellular and
778 intracellular rhizobial infection in Lotus japonicus. *Plant Physiol*, **185**, 1131-1147.
779 **Mun, T., Bachmann, A., Gupta, V., Stougaard, J. and Andersen, S.U.** (2016) Lotus Base: An integrated
780 information portal for the model legume Lotus japonicus. *Sci Rep*, **6**, 39447.
781 **Oldroyd, G.E., Murray, J.D., Poole, P.S. and Downie, J.A.** (2011) The rules of engagement in the
782 legume-rhizobial symbiosis. *Annu Rev Genet*, **45**, 119-144.
783 **Park, S.H., Li, F., Renaud, J., Shen, W., Li, Y., Guo, L., Cui, H., Sumarah, M. and Wang, A.** (2017)
784 NbEXPA1, an alpha-expansin, is plasmodesmata-specific and a novel host factor for potyviral
785 infection. *Plant J*, **92**, 846-861.
786 **Pfaffl, M.W.** (2001) A new mathematical model for relative quantification in real-time RT-PCR.
787 *Nucleic Acids Res*, **29**, e45.
788 **Quilbe, J., Montiel, J., Arrighi, J.F. and Stougaard, J.** (2022) Molecular Mechanisms of Intercellular
789 Rhizobial Infection: Novel Findings of an Ancient Process. *Front Plant Sci*, **13**, 922982.
790 **Radutoiu, S., Madsen, L.H., Madsen, E.B., Felle, H.H., Umehara, Y., Gronlund, M., Sato, S.,**
791 **Nakamura, Y., Tabata, S., Sandal, N. and Stougaard, J.** (2003) Plant recognition of symbiotic
792 bacteria requires two LysM receptor-like kinases. *Nature*, **425**, 585-592.
793 **Rich, M.K., Schorderet, M. and Reinhardt, D.** (2014) The role of the cell wall compartment in
794 mutualistic symbioses of plants. *Front Plant Sci*, **5**, 238.
795 **Roy, S., Liu, W., Nandety, R.S., Crook, A., Mysore, K.S., Pislariu, C.I., Frugoli, J., Dickstein, R. and**
796 **Udvardi, M.K.** (2020) Celebrating 20 Years of Genetic Discoveries in Legume Nodulation and
797 Symbiotic Nitrogen Fixation([OPEN]). *Plant Cell*, **32**, 15-41.
798 **Rubsam, H., Kronauer, C., Abel, N.B., Ji, H., Lironi, D., Hansen, S.B., Nadzieja, M., Kolte, M.V., Abel,**
799 **D., de Jong, N., Madsen, L.H., Liu, H., Stougaard, J., Radutoiu, S. and Andersen, K.R.** (2023)
800 Nanobody-driven signaling reveals the core receptor complex in root nodule symbiosis.
801 *Science*, **379**, 272-277.
802 **Sprent, J.I., Ardley, J. and James, E.K.** (2017) Biogeography of nodulated legumes and their nitrogen-
803 fixing symbionts. *New Phytol*, **215**, 40-56.
804 **Su, C., Zhang, G., Rodriguez-Franco, M., Hinnenberg, R., Wietschorke, J., Liang, P., Yang, W., Uhler,**
805 **L., Li, X. and Ott, T.** (2023) Transcellular progression of infection threads in Medicago
806 truncatula roots is associated with locally confined cell wall modifications. *Curr Biol*, **33**, 533-
807 542 e535.

Wang, Z., Cao, J., Lin, N., Li, J., Wang, Y., Liu, W., Yao, W. and Li, Y. (2024) Origin, Evolution, and Diversification of the Expansin Family in Plants. *Int J Mol Sci*, **25**.

Xie, F., Murray, J.D., Kim, J., Heckmann, A.B., Edwards, A., Oldroyd, G.E. and Downie, J.A. (2012) Legume pectate lyase required for root infection by rhizobia. *Proc Natl Acad Sci U S A*, **109**, 633-638.

Zarrabian, M., Montiel, J., Sandal, N., Ferguson, S., Jin, H., Lin, Y.Y., Klingl, V., Marin, M., James, E.K., Parniske, M., Stougaard, J. and Andersen, S.U. (2022) A promiscuity locus confers Lotus burttii nodulation with rhizobia from five different genera. *Mol Plant Microbe Interact*.

Zhang, G. and Ott, T. (2024) Cellular morphodynamics and signaling around the transcellular passage cleft during rhizobial infections of legume roots. *Curr Opin Cell Biol*, **91**, 102436.

Zhao, L., Ji, C.Y., Murray, J.D. and Liu, C.W. (2025) A legume cellulase required for rhizobial infection and colonization in root nodule symbiosis. *Nat Commun*, **16**, 6663.

A

Gene	*M. loti* 1 dpi	*M. loti* 3 dpi	IRBG74 3 dpi	IRBG74 5 dpi	IRBG74 10 dpi
LotjaGi1g1v0089200					
LotjaGi1g1v0099800					
LotjaGi1g1v0106800					
LotjaGi1g1v0220500					
LotjaGi1g1v0307600					
LotjaGi1g1v0505000					
LotjaGi1g1v0510200					
LotjaGi1g1v0510300					
LotjaGi1g1v0510400					
LotjaGi1g1v0510600					
LotjaGi1g1v0510700					
LotjaGi1g1v0575800					
LotjaGi1g1v0580000					
LotjaGi1g1v0606600					
LotjaGi1g1v0685400					
LotjaGi2g1v0260200					
LotjaGi2g1v0302000					
LotjaGi2g1v0373800					
LotjaGi2g1v0419100					
LotjaGi2g1v0429600					
LotjaGi3g1v0049100					
LotjaGi3g1v0225600					
LotjaGi3g1v0443400					
LotjaGi3g1v0443500					
LotjaGi3g1v0455500					
LotjaGi3g1v0533600					
LotjaGi4g1v0191100					
LotjaGi4g1v0195900					
LotjaGi4g1v0196100					
LotjaGi4g1v0196300					
LotjaGi4g1v0217400					
LotjaGi4g1v0245800					
LotjaGi4g1v0250200					
LotjaGi5g1v0003400					
LotjaGi5g1v0236000					
LotjaGi6g1v0042100					
LotjaGi6g1v0052100					

-2 2

Fold Change

B

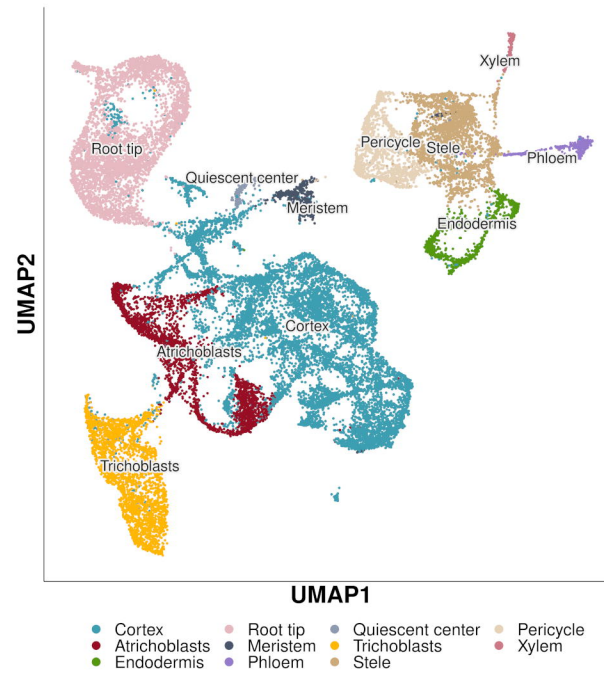

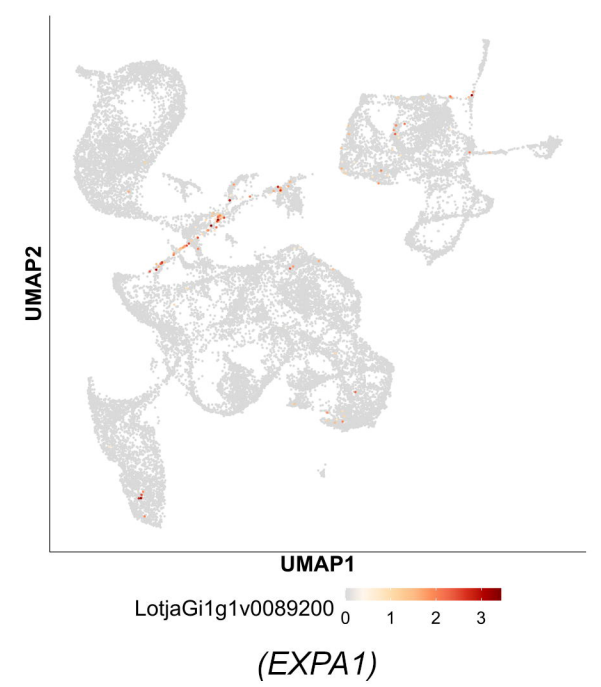

C

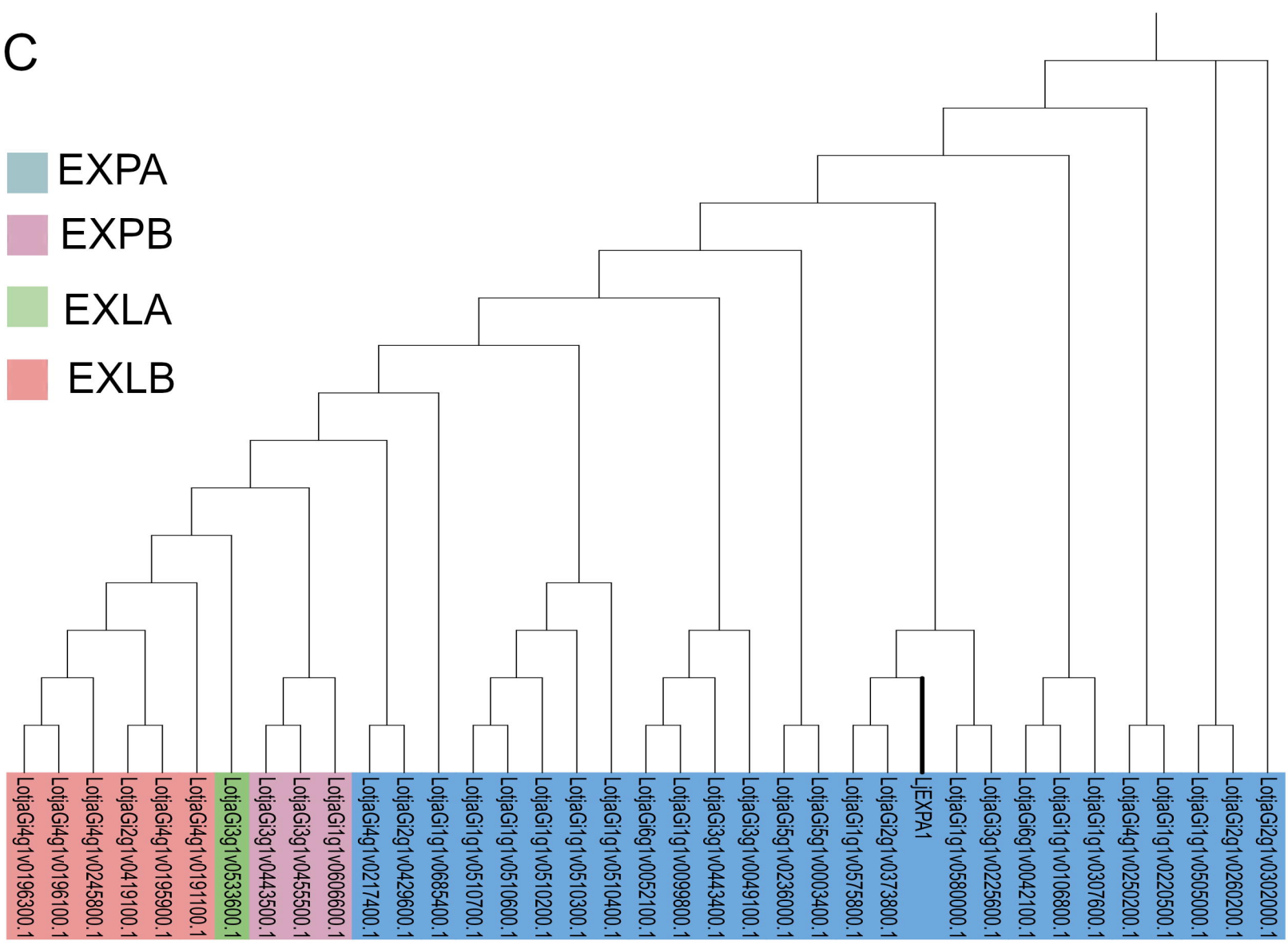

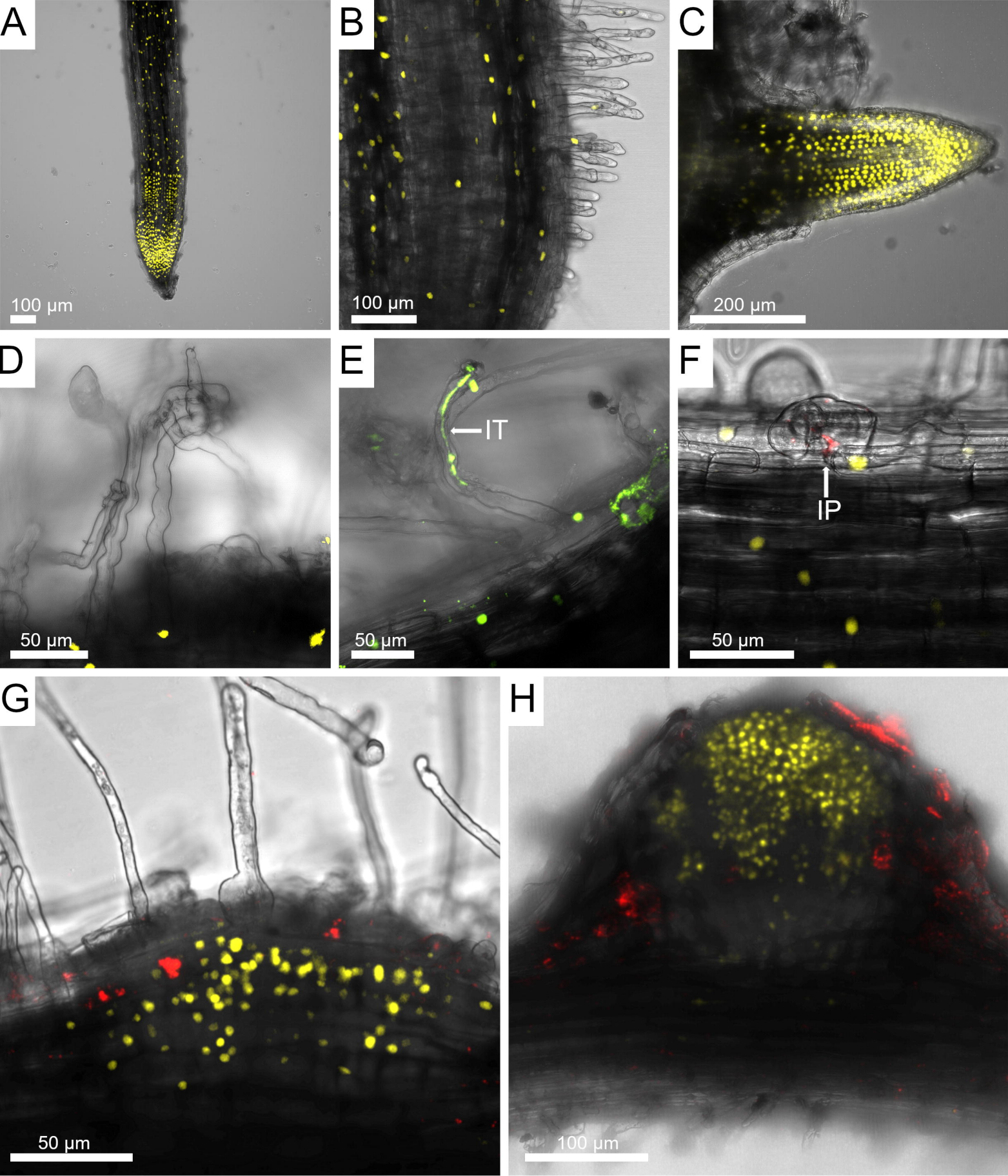
A
100 µm
B
100 µm
C
200 µm
D
50 µm
E
IT
50 µm
F
IP
50 µm
G
50 µm
H
100 µm

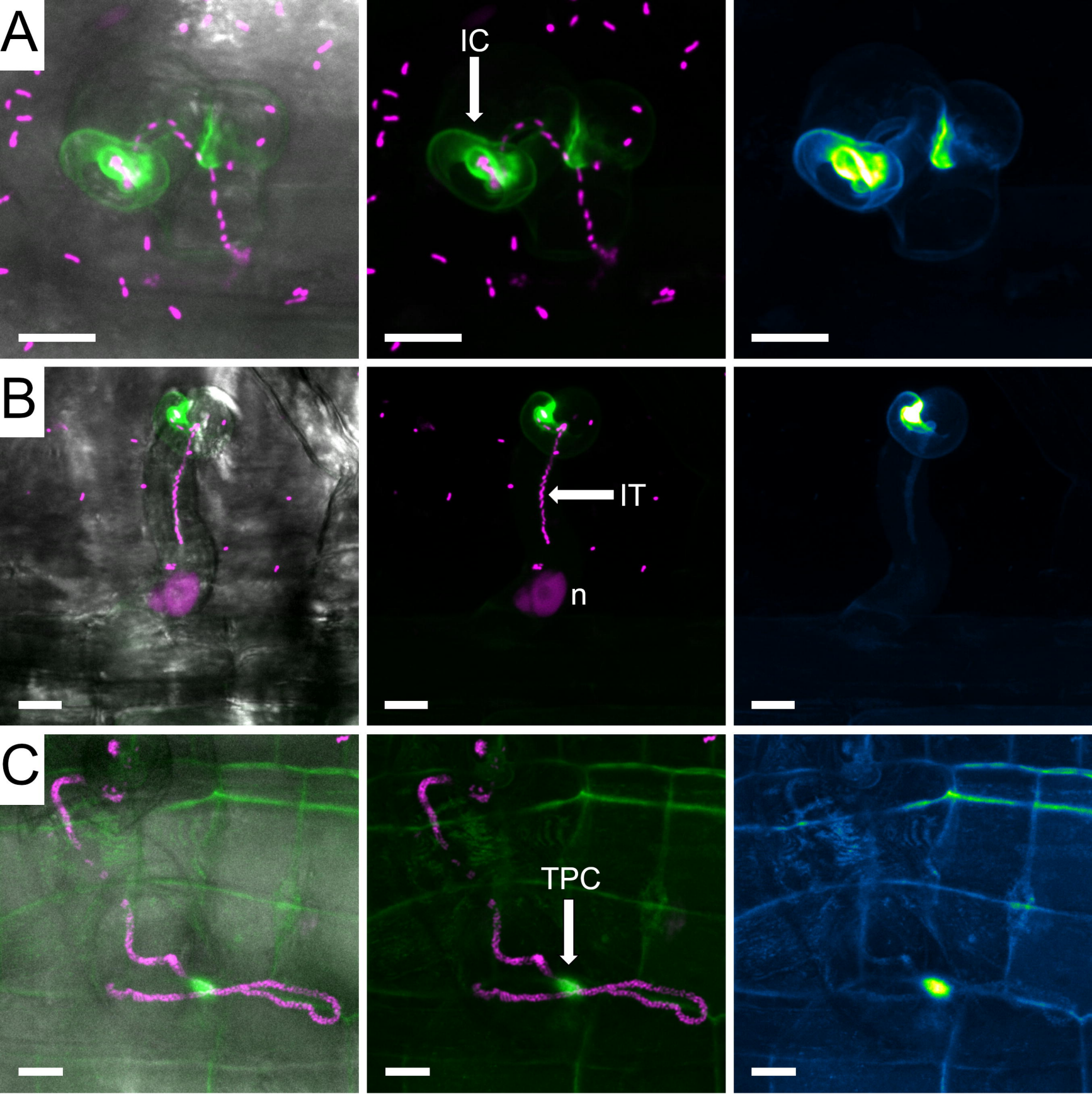
A
IC
B
IT
n
C
TPC
YFP+DsRed + BF
YFP+DsRed
YFP

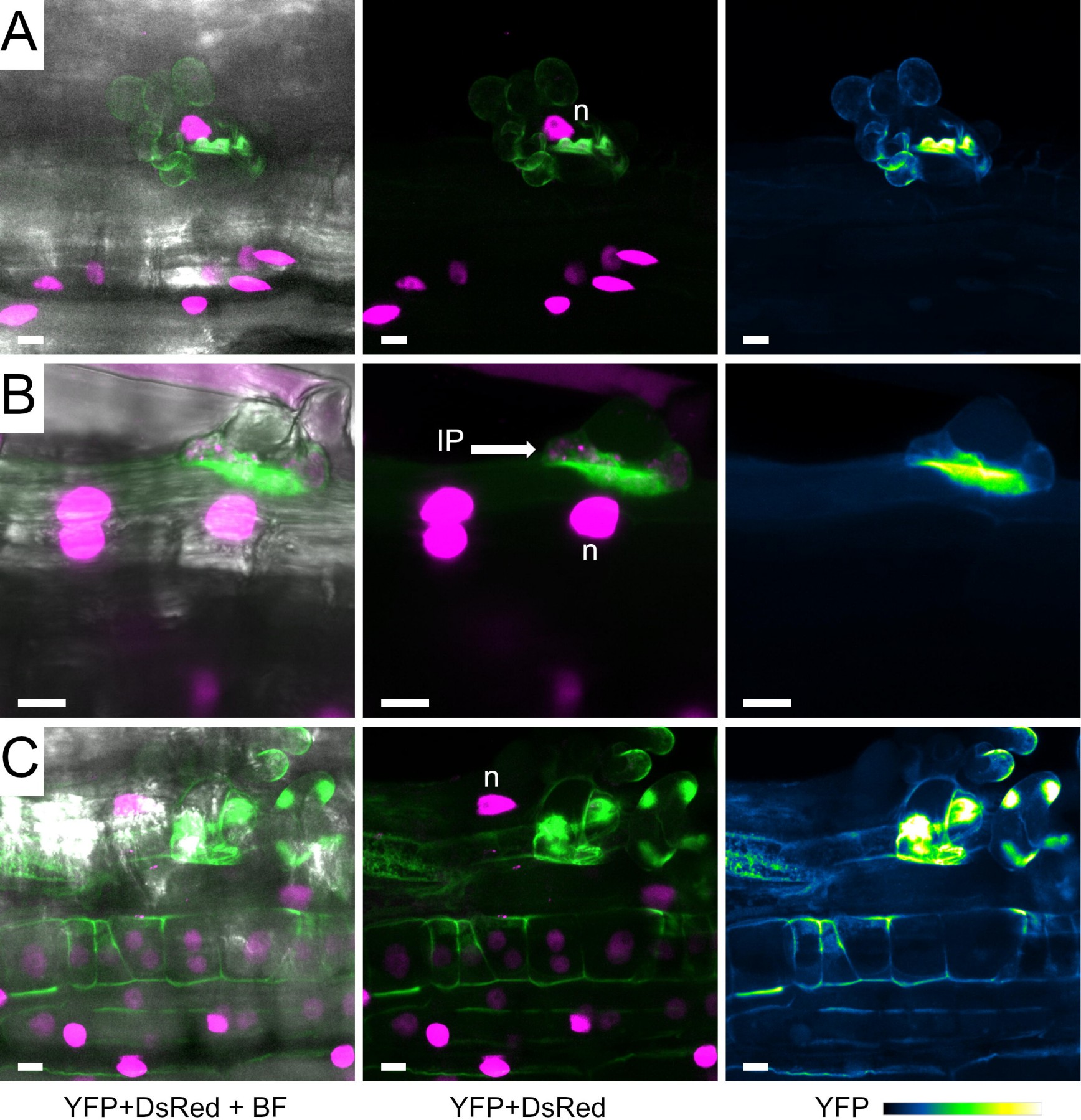
A
n
B
IP
n
C
n
YFP+DsRed + BF
YFP+DsRed
YFP

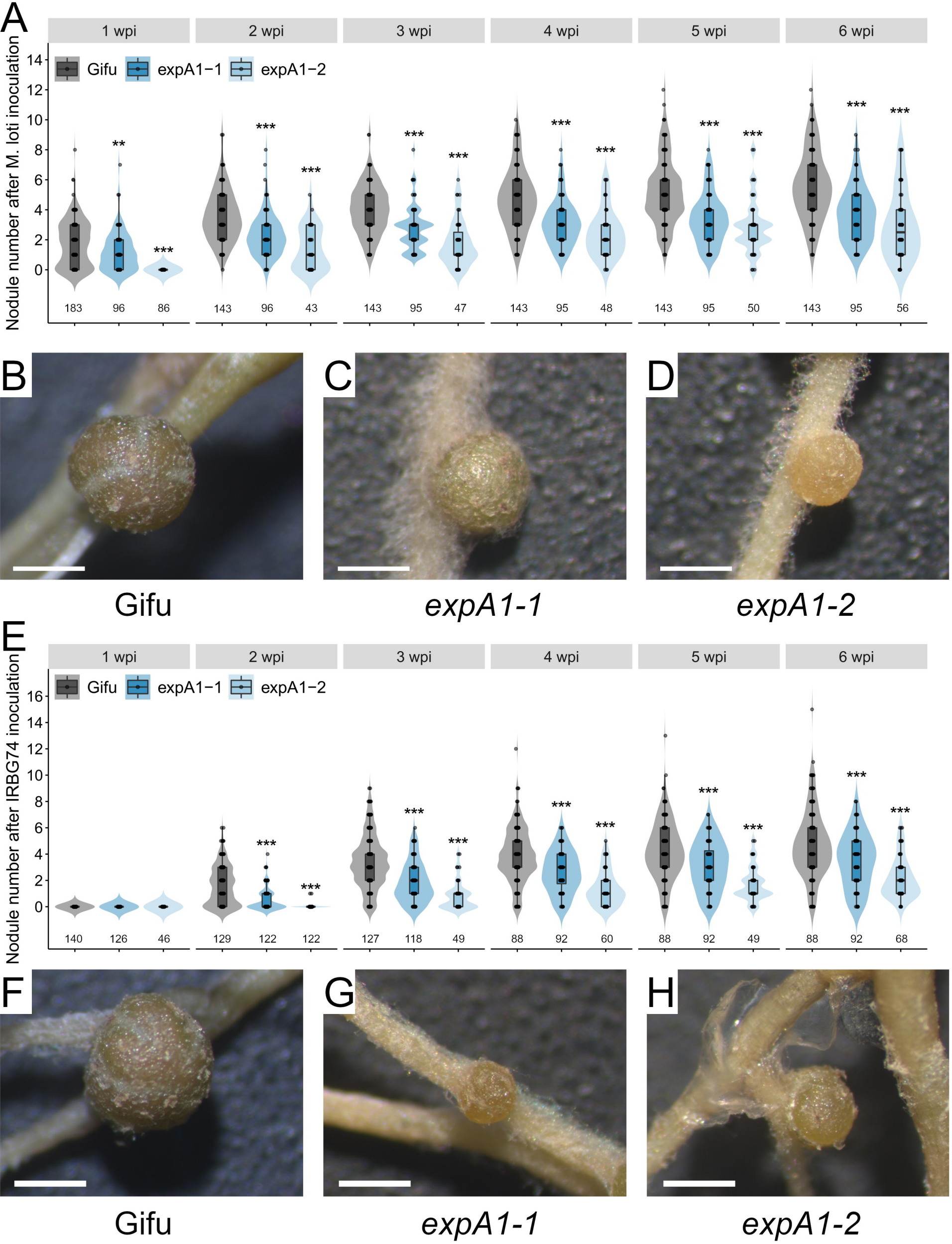
A
1 wpi
2 wpi
3 wpi
4 wpi
5 wpi
6 wpi
Gifu
expA1−1
expA1−2
Nodule number after M. loti inoculation
183 96 86
143 96 43
143 95 47
143 95 48
143 95 50
143 95 56
B
C
D
Gifu
expA1-1
expA1-2
E
Nodule number after IRBG74 inoculation
140 126 46
129 122 122
127 118 49
88 92 60
88 92 49
88 92 68
F
G
H
Gifu
expA1-1
expA1-2

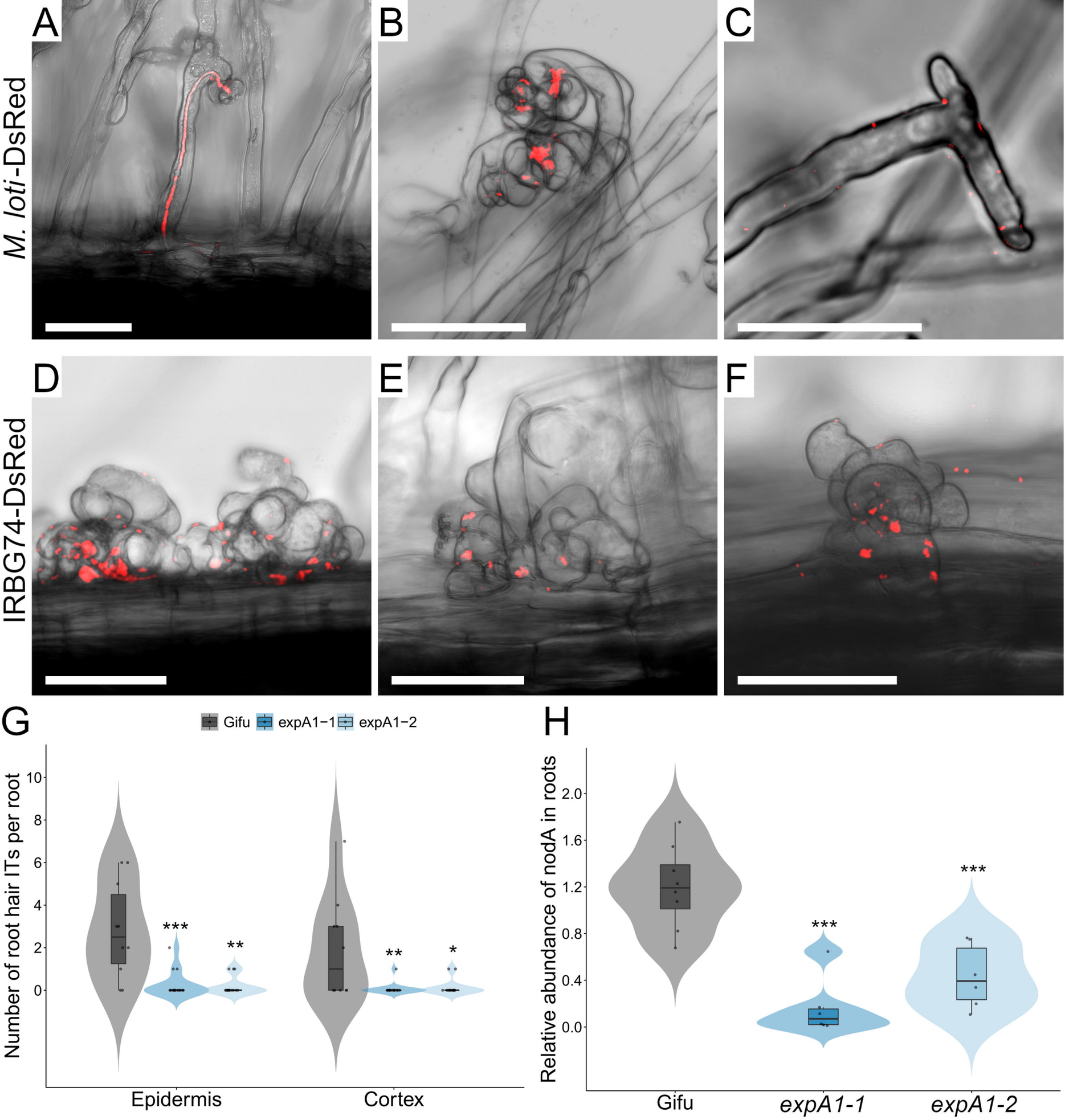
A
B
C
M. loti-DsRed
D
E
F
IRBG74-DsRed
G
Gifu
expA1−1
expA1−2
Number of root hair ITs per root
10
8
6
4
2
0
***
**
**
*
Epidermis
Cortex
H
Relative abundance of nodA in roots
2.0
1.6
1.2
0.8
0.4
0.0
***
***
Gifu
expA1-1
expA1-2